MicroRNAs-103/107 coordinately regulate macropinocytosis and autophagy

Jong Kook Park,[1]* Han Peng,[1]* Julia Katsnelson,[4] Wending Yang,[1] Nihal Kaplan,[1] Ying Dong,[1,5] Joshua Z. Rappoport,[3] CongCong He,[2] and Robert M. Lavker[1]

[1]Department of Dermatology, [2]Department of Cell and Molecular Biology, and [3]Center for Advanced Microscopy and Nikon Imaging Center, Northwestern University, Chicago, IL 60611
[4]Rush Medical Center, Chicago, IL 60615
[5]Department of Ophthalmology, The First Affiliated Hospital, Chinese PLA General Hospital, Beijing 100048, China

Macropinocytosis, by which cells ingest large amounts of fluid, and autophagy, the lysosome-based catabolic process, involve vesicular biogenesis (early stage) and turnover (end stage). Much is known about early-stage events; however, our understanding of how the end stages of these processes are governed is incomplete. Here we demonstrate that the microRNA-103/107(miR-103/107) family, which is preferentially expressed in the stem cell–enriched limbal epithelium, coordinately regulates aspects of both these activities. Loss of miR-103/107 causes dysregulation of macropinocytosis with the formation of large vacuoles, primarily through up-regulation of Src, Ras, and Ankfy1. Vacuole accumulation is not a malfunction of early-stage autophagy; rather, miR-103/107 ensure proper end-stage autophagy by regulating diacylglycerol/protein kinase C and cyclin-dependent kinase 5 signaling, which enables dynamin to function in vacuole clearance. Our findings unveil a key biological function for miR-103/107 in coordinately suppressing macropinocytosis and preserving end-stage autophagy, thereby contributing to maintenance of a stem cell–enriched epithelium.

Introduction

The cornea is a remarkable system in that it must protect the delicate understructures of the eye as well as maintain transparency for proper vision. These two functions are accomplished via an integrated system of an avascular and relatively acellular stroma, which forms the foundation for a stratified squamous epithelium that anchors the tear film (Lavker et al., 1991). By virtue of interfacing with the external environment, the corneal epithelium is in a steady state, constantly losing cells, which must be replaced in an orderly fashion (Lavker et al., 2004). Such self-renewing epithelia are, by definition, governed by stem cells; however, the corneal epithelium is unique because its stem cell population is preferentially located in the adjacent limbal epithelium (Schermer et al., 1986; Cotsarelis et al., 1989). Consequently, the corneal epithelium is enriched in the progeny (transit-amplifying [TA] cells) of the limbal-derived epithelial stem cells (Lehrer et al., 1998). This physical separation between stem and TA cells makes the corneal/limbal epithelia an ideal model for studying the biological properties of these two proliferative populations (Zhou et al., 2006; Peng et al., 2015). As a result, a plethora of studies have been conducted that help to define the limbal stem cell and its biological properties (Lavker et al., 2004; Schlötzer-Schrehardt and Kruse, 2005; Stepp and Zieske, 2005; Davies and Di Girolamo, 2010; Li et al., 2014; Peng et al., 2015).

Autophagy is an essential means by which cells adapt to differing intrinsic and extrinsic cellular stress-related situations (Eskelinen and Saftig, 2009). Stem cells are long-lived and capable of self-renewal and quiescence (Lavker and Sun, 2000), properties requiring active elimination of unnecessary proteins and organelles that accumulate during stem cell homeostasis (Salemi et al., 2012; Phadwal et al., 2013). Most investigations into stem cells and autophagy have focused on either embryonic or adult hematopoietic, mesenchymal, or neuronal stem cells (Phadwal et al., 2013). Conspicuous by their absence are investigations directed at autophagy in the limbal epithelium, the site of corneal epithelial stem cells (Schermer et al., 1986; Cotsarelis et al., 1989). Equally remarkable is the scant attention that has been paid to autophagy in the corneal epithelium. The exceptions are recent studies in cultured human corneal epithelial cells demonstrating that lacritin, a tear-derived epithelial mitogen (Sanghi et al., 2001), acetylates FOXO3 (Wang et al., 2013). Such acetylation results in a coupling with ATG101 and the subsequent initiation of autophagy (Wang et al., 2013). Although the initiation of autophagy has been well studied in

*J.K. Park and H. Peng contributed equally to this paper.

Correspondence to Robert M. Lavker: r-lavker@northwestern.edu

Abbreviations used: ALR, autophagic lysosome reformation; CDK5, cyclin-dependent kinase 5; HLEK, human limbal epithelial keratinocyte; HSC, hematopoietic stem cell; LC3, light chain 3; mTOR, mechanistic target of rapamycin; PA, phosphatidic acid; PLD1, phospholipase D1; SIM, structured illumination microscopy; TA, transit-amplifying; TEM, transmission electron microscopy.

The Rockefeller University Press $30.00
J. Cell Biol. Vol. 215 No. 5 667–685
https://doi.org/10.1083/jcb.201604032

a variety of systems, the late stages of autophagy have been relatively neglected (Chen and Yu, 2013).

Equally understudied in the limbal/corneal epithelia are events associated with macropinocytosis, the clathrin-independent endocytic process resulting in the formation of large (0.2 to 2 µm) macropinosomes (Lim and Gleeson, 2011; Maltese and Overmeyer, 2015). Macropinocytosis enables cells to nonselectively engulf and take up large volumes of fluid and membrane via the closure of plasma membrane protrusions (Lewis, 1931; Lim and Gleeson, 2011). Membrane ruffling with its associated remodeling of the cytoskeleton appears to be required for macropinocytosis, but not sufficient for macropinosome formation (Araki et al., 1996; West et al., 2000). Once formed, macropinosomes undergo a maturation process and are either degraded via a late endosome/lysosome process or recycled back to the plasma membrane (Lim and Gleeson, 2011). Precise signaling events are unclear, as is how components of macropinocytosis are coordinated; however, macropinocytosis is likely to be distinctive in different cell types (Lim and Gleeson, 2011; Maltese and Overmeyer, 2015). Interestingly, one of the morphological features of dysregulation of macropinocytosis is the appearance of large cytoplasmic vacuoles (Overmeyer et al., 2011; Maltese and Overmeyer, 2015).

A recently described, limbal epithelial–preferred miRNA family, miR-103/107, regulates and integrates limbal keratinocyte cell cycle quiescence, proliferative capacity, and cell–cell communication, processes that are intimately involved in stem cell maintenance (Peng et al., 2015). We now report that miR-103/107 not only regulate aspects of macropinocytosis and autophagy but serve to coordinate these two processes to maintain limbal epithelial homeostasis. Limbal keratinocytes deficient in this miRNA family rapidly develop large hollow vacuoles that originate, in part, from a dysregulation in macropinocytosis. We demonstrate that the loss of miR-103/107 increases Src/Ras, which initiates vacuole formation through macropinocytosis. Such miRNA loss also up-regulates the Rab 5 effector, ANKFY1, which is essential for macropinocytosis (Schnatwinkel et al., 2004). Once vacuoles are formed, their size continuously increases. Initiation of autophagosome formation, lysosomal fusion, and pH are not compromised in these cells, suggesting a defect in vacuole clearance. Loss of miR-103/107 increases dynamin phosphorylation (inactivation), which retards endocytic processes (Powell et al., 2000). This ultimately results in a failure of dynamin binding with vacuoles and a defect in end-stage autophagy. Collectively, our findings provide new insight into how macropinocytosis and autophagy are coordinately regulated in a stem cell–enriched epithelium.

Results

Loss of miR-103/107 induces formation of hollow vacuoles

It has been shown that after the knockdown of miR-103/107 by antagomir treatment in primary human limbal keratinocytes (HLEKs) and in a human limbal-derived epithelial cell line (hTCEpi), cells rapidly separate from each other (Peng et al., 2015). This antagomir approach specifically silenced miR-103/107 without affecting the expression of other corneal/limbal-associated miRNAs such as miR-31, miR-184, and miR-205 (Fig. S1 A; Peng et al., 2015). These cells are characterized by the presence of numerous, large vacuoles (Fig. 1 A) that increase in diameter with time (mean diameter 10–16 µm; Fig. 1 B). Examination of these cells by transmission electron microscopy (TEM) revealed that the large vacuoles were markedly devoid of cellular material and were enveloped by a single membrane. On the internal surface of the vesicle membrane, deposition of membranous material was frequently seen to be organized into small vesicles or myelin-like figures (Fig. 1 C). In contrast, control (antago-124–treated) HLEKs had few, if any, hollow vacuoles but did contain numerous lysosomes, lipid droplets, and autophagosomes, as indicated by double membranes (Fig. 1 C). TEM images showed that the vacuoles frequently appeared close to the nucleus; however, despite their large size relative to the cell, a compaction of organelles (e.g., mitochondria, Golgi, and rough ER) in the cytoplasm adjacent to the vacuoles was not observed (Figs. 1 C and S1 B). It should be noted that we did not see evidence of cell death as assessed by (a) lack of viability; (b) light microscopic detection of fragmented cells or cell debris; and (c) ultrastructural evidence of necrosis, after 72 h of treatment with antago-103/107 (unpublished data).

To determine the nature of these vacuoles, we used immunostaining to localize several markers of lysosomes, autophagosomes, and endosomes. Confocal microscopy showed a colocalization of LAMP1 (a lysosomal marker [Rohrer et al., 1996]) and Lysotracker (an indicator of acidification [Freundt et al., 2007]; red color) on the vacuoles in the antago-103/107–treated HLEKs (Fig. 2 A). To examine further the association of these markers with the vacuoles, superresolution structured illumination microscopy (SIM) was conducted. The results clearly showed a colocalization of LAMP1 and Lysotracker with the vacuole (Fig. 2 B). Furthermore, line scan analysis (Fig. 2 B) indicated no other LAMP1/LysoTracker-positive structures within 1 µm surrounding the vacuole, which is consistent with the TEM observations showing no organelle compaction around the vacuoles (Figs. 1 C and S1 B). Vacuoles did not express the early endosomal marker EEA1 (Fig. 2 C). These vacuoles incorporated the macropinosome marker Lucifer yellow (Fig. 3, A and B). Collectively, these images suggest that loss of miR-103/107 causes the accumulation of large vacuoles and implicates macropinocytosis as a possible initiating mechanism.

Loss of miR-103/107 triggers dysregulation of macropinocytosis

To identify miRNA targets in an unbiased manner, we knocked down miR-103/107 in HLEKs using antagomirs and conducted mRNA profiling combined with bioinformatic analysis (Peng et al., 2015). In such an analysis, apoptosis, metabolic processes, and response to stress were major biological events predicted to be affected by miR-103/107 (Fig. S1 C). To begin to understand the mechanisms underlying the formation of the vacuoles, we used a pharmacological approach, whereby we cotreated HLEKs for 24 h with antago-103/107 and a variety of pharmacological inhibitors (Fig. S1 D; and Table S1). The presence of vacuoles after such treatment was used as an indicator of efficacy. In general, inhibitors of apoptosis (e.g., Z-VAD-FMK [caspase] and EUK134 [ROS]) failed to block vacuole formation (Fig. S1 E). The most dramatic blockage (>95%) of the vacuoles was observed after treatment of either HLEKs or hTCEpi cells with amiloride (Fig. 3, C and D) and its derivative, 5-(*N*-ethyl-*N*-isopropyl)amiloride (EIPA; Fig. 3 E), which uniquely inhibits macropinosome formation (Koivusalo et al., 2010). Src and Ras are involved in the induction of macropinocytosis (Lim and Gleeson, 2011; Maltese and Overmeyer, 2015). Therefore, it is

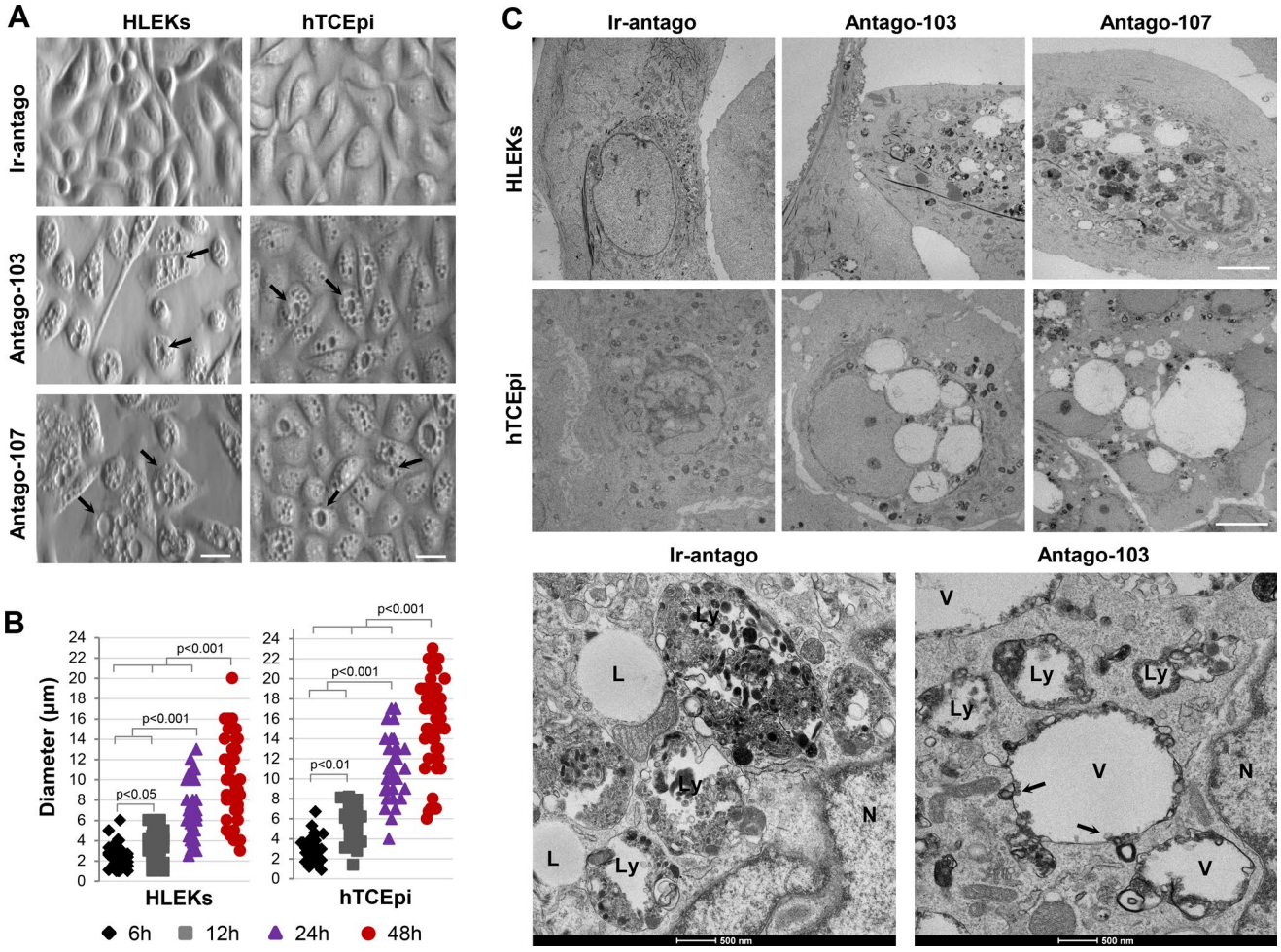

Figure 1. **Loss of miR-103/107 results in vacuole formation.** (A) Phase-contrast microscopy of primary HLEKs and hTCEpi cells 24 h after treatment with ir-antago, antago-103, or antago-107. Antago-103/107 treatment causes numerous large vacuoles (arrows). Bars, 20 μm. (B) Time course measurements of vacuole diameter in HLEKs and hTCEpi cells after treatment with antago-103/107 mixture (n = 30 vacuoles/time point). (C) Representative TEM images of HLEKs and hTCEpi cells 24 h after treatment with ir-antago, antago-103, or antago-107. Representative high-magnification TEM images (bottom) show lipid droplets (L), lysosomes (Ly), and vacuoles (V). Note the deposition of membranous material on the inside of the vacuoles (arrows). N, nucleus. Bars, 5 μm.

not surprising that loss of miR-103/107 activates Src and Ras (Fig. 3, F and G), and inhibitors of the Src and Ras families (i.e., PP2 or manumycin) strongly blocked vacuole formation (Fig. 3, H and I). Using a genetic approach, we demonstrated that knockdown of Src or Ras also blocked vacuole formation (Fig. 3, J and K). Further evidence for the involvement of macropinocytosis in the formation of the vacuoles is that cotreatment of HLEKs and hTCEpi cells with antago-103/107 and the Rac inhibitor NSC23766 or the Cdc42 inhibitor ZCL278 blocked vacuole formation (Fig. S2, A and B). Knockdown of Rac1 and Cdc42 similarly blocked vacuole formation (Fig. S2, C and D). Rac1 and Cdc42 are required for optimal macropinocytosis, and amiloride abrogates their signaling, thus interfering with macropinocytosis (Koivusalo et al., 2010). To assess biochemically whether antago-103/107 preferentially affect Rac1 or Cdc42 activation, HLEKs were treated with antago-103/107, and the active forms of Rac1 and Cdc42 were pulled down and immunoblotted with Rac1- or Cdc42-specific antibodies (Fig. S2 E). Both Rac1 and Cdc42 were activated by antago-103/107 (Fig. S2 E). This is strong evidence that macropinocytosis is an initiating factor in vacuole formation.

miR-103/107 family regulates macropinocytosis by targeting SHC3 and ANKFY1

SHC3 is an adaptor protein that is associated with activation of the RAS/MAPK signaling pathway (Li et al., 2007). *SHC3* has a 3′ UTR seed sequence that binds to miR-103/107 (Fig. S2 F), making it a putative target. Luciferase assays in combination with immunoblotting confirmed the target prediction (Fig. S2 G), as SHC3 protein was markedly diminished in HLEKs treated with miR-103/107 (Fig. 4 B). Conversely, treatment of HLEKs and hTCEpi with antago-103/107 clearly up-regulated SHC3 levels (Fig. 4 C). This is strong evidence that *SHC3* is a target of miR-103/107.

ANKFY1 (also known as rabankyrin-5) is a novel Rab5 FYVE-finger effector that localizes to macropinosomes and, together with Rab5, is required for macropinocytosis (Schnatwinkel et al., 2004). Interestingly, *ANKFY1* is a predicted target of miR-103/107, and this was confirmed by luciferase assays (Fig. S2, F and G). Overexpression of miR-103/107 in HLEKs significantly decreased ANKFY1 levels (Fig. 4 D), whereas knockdown of miR-103/107

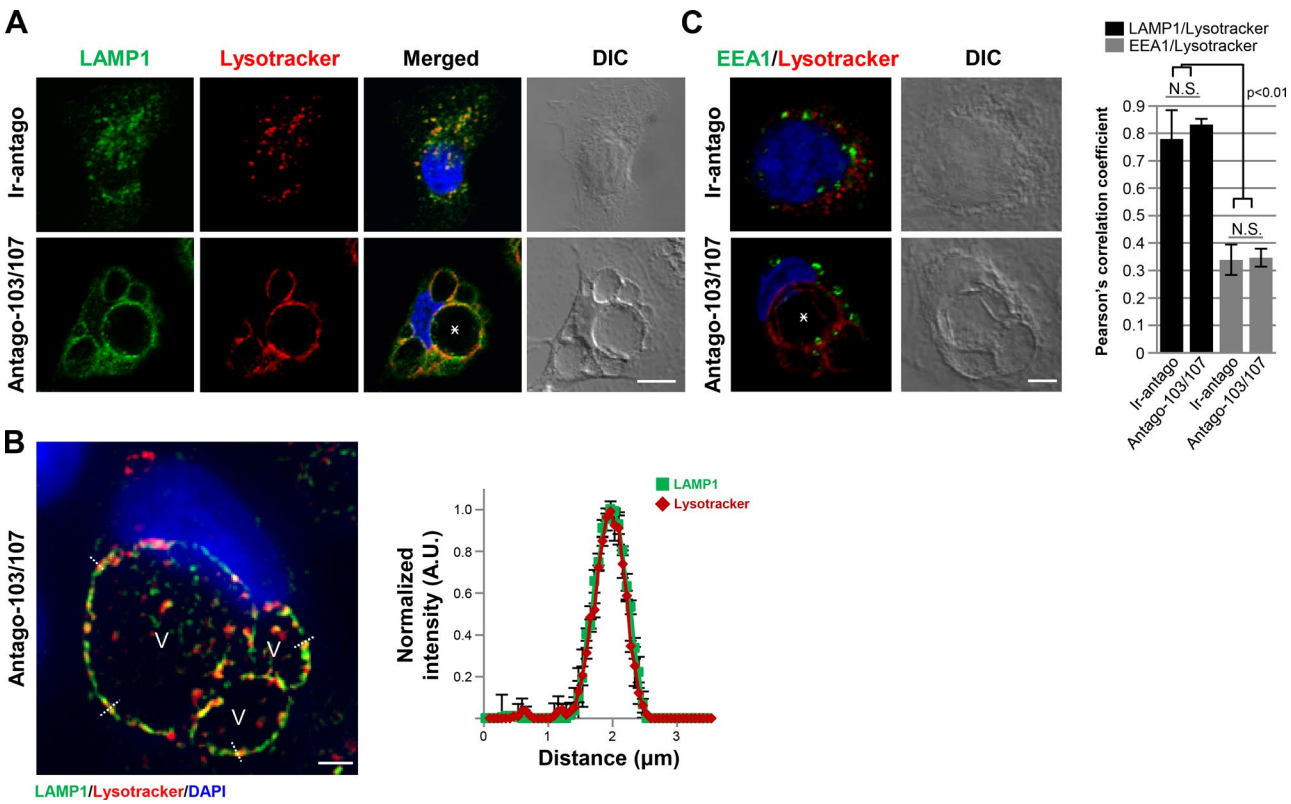

Figure 2. **Lysosomal markers are colocalized on vacuoles.** (A) Double staining of antago-103/107–treated HLEKs at 24 h with LysoTracker Red (DND-99) and lysosomal-associated membrane protein 1 (LAMP1; green). Asterisk indicates a representative vacuole. Bar, 10 µm. (B) SIM image shows colocalization of LAMP1 and Lysotracker on the vacuoles. Line scan analysis was conducted (dashed white lines). V, vacuoles. A.U., arbitrary unit. Bar, 5 µm. (C) HLEKs stained for intracellular EEA1 and LysoTracker Red (DND-99) 24 h after treatment with ir-antago or antago-103/107. Asterisk indicates a representative vacuole. Pearson's correlation coefficient analysis between LysoTracker Red (DND-99) and LAMP1 or EEA1 in ir-antago or antago-103/107 HLEKs is shown in the bar graph (n = 12 cells for each). N.S., not statistically significant. Bar, 5 µm. All error bars represent SD.

markedly increased ANKFY1 levels (Fig. 4 E). Consistent with the involvement of macropinocytosis in vacuole formation, ANKFY1 was detected on the periphery of the large antago-103/107–induced vacuoles (Fig. 4 F).

Src activation is sufficient to trigger ruffling and macropinocytosis (Veithen et al., 1996; Mettlen et al., 2006). After treatment of HLEKs and hTCEpi cells with antago-103/107, a marked increase in the docking protein NEDD9 (O'Neill et al., 2000) was observed (Peng et al., 2015). Subsequent analysis revealed that *NEDD9* was a bona fide target of miR-103/107 (Peng et al., 2015). To further confirm that miR-103/107 regulate macropinocytosis through NEDD9, SHC3, and ANKFY1, we knocked down these three proteins in antago-103/107–treated HLEKs and showed that silencing of SHC3 and ANKFY1 rescued vacuole formation (Fig. 4, G and H). Knockdown of NEDD9 did not significantly alter the number of vacuoles (Fig. 4 G) but partially reduced Src activity (Fig. 4 H). This finding supports the interrelationship between NEDD9 and Src kinase (Bradbury et al., 2014; Peng et al., 2015) and further suggests that miR-103/107 regulates Src activity through NEDD9 as well as other genes. Nonetheless, our findings indicate that miR-103/107 regulate macropinocytosis, in part, at two stages. First, by targeting *NEDD9* and *SHC3*, Src and Ras activation are attenuated and the initiation of macropinocytosis is regulated (Fig. 4 A). Second, by targeting *ANKFY1*, miR-103/107 also interfere with the formation of the macropinosome, which contributes to the large vacuoles (Fig. 4 A).

Vacuoles are defective in digesting protein taken up via macropinocytosis

Macropinocytosis is known to supply amino acids into cells by the intracellular uptake of protein (Commisso et al., 2013; Palm et al., 2015). Our Lysotracker labeling data indicated that only the peripheral portion of the vacuole was acidic; the interior of the vacuoles was nonacidic. Therefore, we monitored the proteolytic degradation status of these vacuoles. After loss of miR-103/107, FITC-BSA was used to detect whether the large vacuoles could internalize BSA (Fig. 5 A). To monitor whether the vacuoles were capable of proteolytic degradation of BSA, we used DQ-BSA, which generates red fluorescence by enzymatic cleavage (Ha et al., 2010; Commisso et al., 2013). Red fluorescence was not observed within the large vacuoles (Fig. 5 A), indicating a failure to generate amino acids from macropinocytosis of protein. To confirm this idea, we monitored intracellular glutamate levels after loss of miR-103/107. We observed a temporal decrease in glutamate levels in antago-103/107–treated HLEKs compared with irrelevant antago (ir-antago)–treated cells (Fig. 5 B). After the exogenous addition of BSA to the HLEKs, we observed an increase in glutamate levels in ir-antago–treated cells but not in antago-103/107–treated cells (Fig. 5 C). Although our findings show uptake of proteins via macropinocytosis as well as an explanation for the mechanisms underlying the formation of the large vacuoles, they do not answer the question of why the large vacuoles are retained in the HLEKs and hTECpi cells.

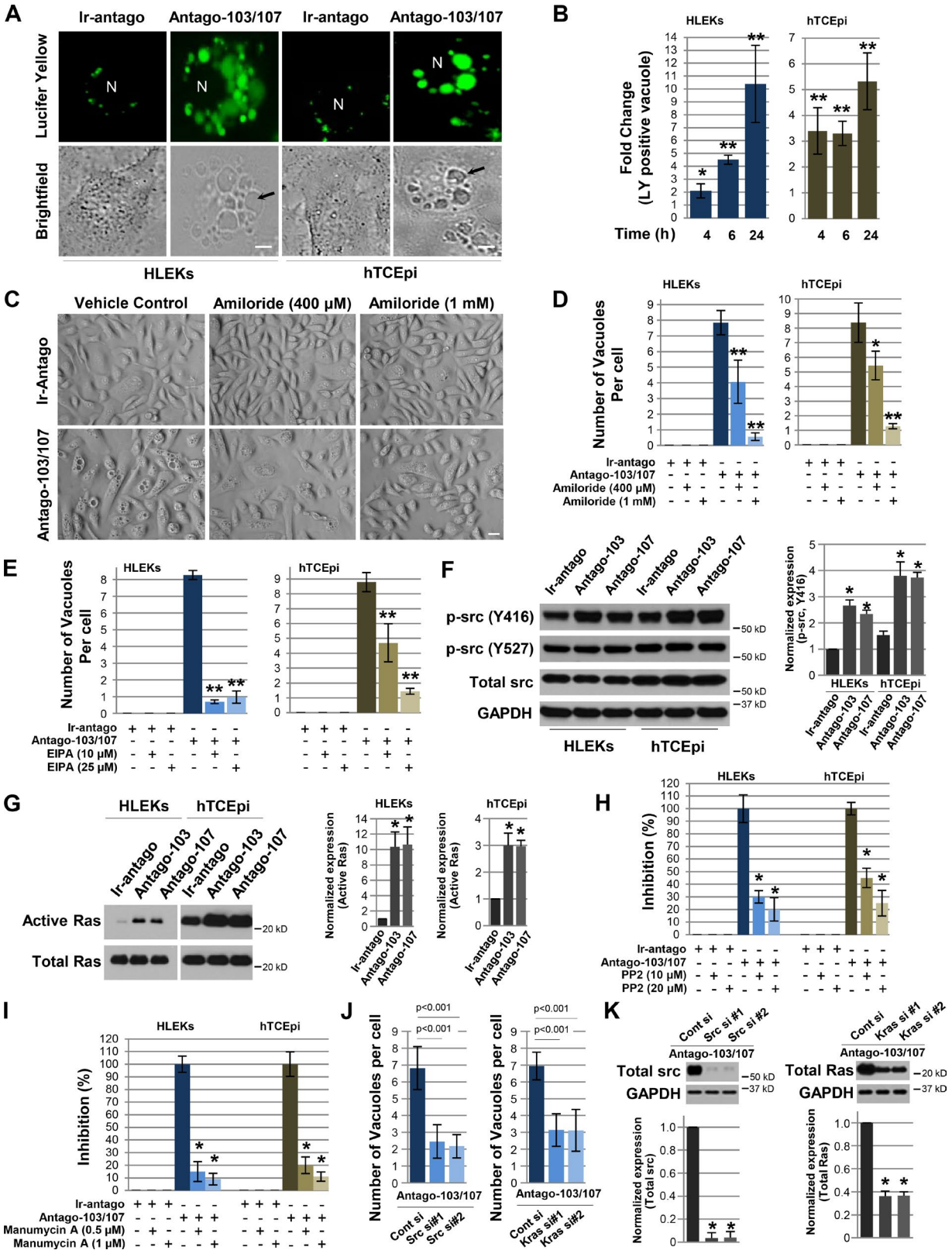

Figure 3. **Loss of miR-103/107 induces macropinocytosis.** (A) After treatment of HLEKs and hTCEpi cells, uptake of the fluid-phase marker, Lucifer Yellow, was noted in the antago-103/107–treated cells. Arrows indicate representative vacuoles in corresponding phase-contrast images (bottom). N, nucleus. Bars, 5 μm. (B) Fold change induction of Lucifer Yellow (LY)-positive vacuoles in HLEKs and hTCEpi cells. The levels of LY-positive vacuoles were calculated relative to the corresponding ir-antago–treated cells, and the data are expressed as fold increase under input control (ir-antago), which was assigned a value of 1. *, $P < 0.01$; **, $P < 0.001$. (C) Representative phase-contrast microscope images of HLEKs treated with ir-antago or antago-103/107 for 24 h with and without amiloride at the indicated concentrations. Bar, 20 μm. (D and E) Inhibitory effects of amiloride and its derivative EIPA on vacuole formation (number of vacuoles) were evaluated in HLEKs and hTCEpi cells. Amiloride (D) and EIPA (E) treatment at two indicated concentrations markedly inhibits the

Vacuoles have morphogenetic characteristics associated with autophagy

The morphology of the vacuoles formed in response to the loss of miR-103/107 as revealed by light microscopy and TEM (Fig. 1, A and C) was similar to that of lysosomal structures reported in a variety of autophagic situations (Caplan et al., 2001; Martinet et al., 2007; Chen et al., 2011; Ling and Salvaterra, 2011; Gukovskaya and Gukovsky, 2012; Juopperi et al., 2012). Thus we investigated the possibility that the vacuoles were also associated with autophagy. Microtubule-associated protein light chain 3 (LC3) and its family members are retained inside autophagosomes, and thus LC3 is commonly used as a marker for identifying autophagosomes (Barth et al., 2010; Klionsky et al., 2012; Lamb et al., 2013; Phadwal et al., 2013). Immunostaining of antago-103/107–treated HLEKs with LC3 and Lysotracker (a lysosomal marker) showed colocalization of these two markers around the large vacuoles (Fig. 6, A and C). Similar colocalization of Lysotracker and Rab11, a marker of autophagosome maturation (Chua et al., 2011), was observed on the large vacuoles (Fig. 6, B and C). Furthermore, super-resolution SIM confirmed that LC3/Lysotracker (Fig. 6, D and F) and Rab11/Lysotracker (Fig. 6, E and G) were colocalized with the vacuoles. This suggests that miR-103/107 may be involved in autophagy.

Vacuoles represent a defect in end-stage autophagy

We next turned our attention to where in the autophagic process miR-103/107 had the greatest effect. Bafilomycin A1 (BafA1) disrupts vesicular proton gradients (Yoshimori et al., 1991) and prevents the fusion of autophagosomes with lysosomes (Yamamoto et al., 1998). This in turn inhibits autophagy. Thus we used this drug to establish whether vacuole accumulation occurred during early or late stages of autophagy. After 1- or 24-h treatment of HLEKs with BafA1, we saw a marked reduction in antago-103/107–induced large vacuoles at both time points, indicating that the formation of such vacuoles is downstream of lysosome fusion and hence an end-stage event (Fig. 7 A and Fig. S3 A). TEM of ir-antago– and antago-103/107–treated HLEKs exposed to BafA1 revealed morphologically identical autophagolysosomes, some of which contained mitochondrial remnants typical of autophagy (Figs. 7 B and S3 B). There was no TEM evidence of large vacuoles in the antago-103/107–treated HLEKs exposed to BafA1 (Figs. 7 B and S3 B). Chloroquine concentrates in lysosomes and disrupts the function of lysosomal enzymes (Boya et al., 2003). Thus we used this drug to interrogate whether vacuole accumulation was an early- or late-stage event. Similar to the BafA1 findings, a decrease in vacuoles was observed after exposure of antago-103/107–treated HLEKs to chloroquine (Fig. 7 C), which reinforces the idea that vacuoles are caused by a defect in end-stage autophagy.

Taking a genetic approach, we knocked down Beclin-1, which is one of the key proteins in the early stages of autophagy (Klionsky et al., 2012), and observed a decrease in vacuolated cells on a background of antago-103/107 treatment (Fig. S3, C and D), confirming the involvement of autophagy in vacuole retention. Furthermore, knockdown of Beclin-1 resulted in an overall decrease in LC3II in both ir-antago– and antago-103/107–treated HLEKs compared with the control shRNA-treated cells (Fig. S3 D). It should be noted that in the HLEKs treated with shRNA targeting Beclin-1 (shBeclin-1), loss of miR-103/107 still increased LC3II (Fig. S3 D), confirming that the presence of vacuoles is an end-stage event.

After treatment of HLEKs with antago-103/107, we did not observe a change in the levels of autophagy-related proteins Atg3, Atg5, Atg7, and Beclin-1 (Fig. S4 A), which are associated with early activation of autophagy (Klionsky et al., 2012; Lamb et al., 2013). Mechanistic target of rapamycin (mTOR) signaling is not required for the initiation of autophagy but appears to be required for late-stage processes such as recycling of protolysosomal membrane components (Yu et al., 2010). We did not detect any changes in the mTOR signaling complex after treatment of HLEKs with antago-103/107 (Fig. S4 B).

Having established that the accumulation of vacuoles is a function of late-stage autophagy, we wanted to determine whether autophagy flux was altered after loss of miR-103/107. To accomplish this, we used two approaches. First, LC3 is commonly used to monitor autophagy, and LC3-II correlates with the number of autophagosomes (Mizushima et al., 2010; Klionsky et al., 2012). However, the amount of LC3-II alone does not indicate flux (Klionsky et al., 2012). Thus, comparing LC3-II levels in the presence and absence of inhibitors of autophagosome–lysosome fusion (e.g., BafA1) is a good indicator of flux (Mizushima et al., 2010; Klionsky et al., 2012). In the antago-103/107–treated HLEKs, the differences in LC3-II expression between vehicle and BafA1 treatments were less compared with the ir-antago treatment (Figs. 7 D and S3 E). This indicates that a smaller amount of LC3-II was delivered to lysosomes for degradation in antago-103/107–treated cells and is strong evidence of autophagic flux inhibition (Mizushima et al., 2010; Klionsky et al., 2012). This is consistent with the accumulation of vacuoles. Second, we monitored the levels of p62, because this protein binds to ubiquitinated proteins in the cytosol and directly interacts with LC3 that is bound to phagosomes (Bjørkøy et al., 2005). In HLEKs treated with antago-103/107, an increase in p62 levels was noted compared with ir-antago treatment (Fig. 7 E). p62 accumulation is an accepted measure of defects in selective autophagy flux (Barth et al., 2010; Mizushima et al., 2010; Klionsky et al., 2012), which is consistent with our autophagy flux data (Figs. 7 D and S3 E).

number of vacuoles in antago-103/107–treated HLEKs and hTCEpi cells (vacuoles/cell; $n = 50$ cells). *, $P < 0.01$; **, $P < 0.001$. (F) Lysates of ir-antago–, antago-103–, or antago-107–treated HLEKs and hTCEpi cells were immunoblotted with anti-phospho-Src (Y416 and Y527) and total Src. Phosphorylation at Y416 (active) is elevated in antago-103/107–treated cells, whereas Y527 phosphorylation (inactive) is stable. Normalized levels of phospho-Src (Y416) to GAPDH are included. *, $P < 0.01$. (G) Pulldown assay was performed to detect active Ras (Ras-GTP) in HLEKs and hTCEpi cells treated with ir-antago, antago-103, or antago-107 for 24 h. Normalized levels of Ras-GTP to total levels are indicated. *, $P < 0.01$. (H and I) Ir-antago or antago-103/107 mixture was simultaneously cotreated with PP2 (H) or manumycin A (I) at indicated concentrations for 24 h. Data are expressed as relative percentage under input control (antago-103/107 + vehicle control), which was assigned a value of 100 ($n = 50$ cells). *, $P < 0.001$. (J and K) The number of vacuoles/cell was determined in Src- or Kras-depleted HLEKs 48 h after treatment with antago-103/107 mixture (J; $n = 50$ cells), and protein lysates were subjected to immunoblotting with antibodies to Src, total Ras, and GAPDH (K). Normalized levels to GAPDH are included. *, $P < 0.01$. All error bars represent SD.

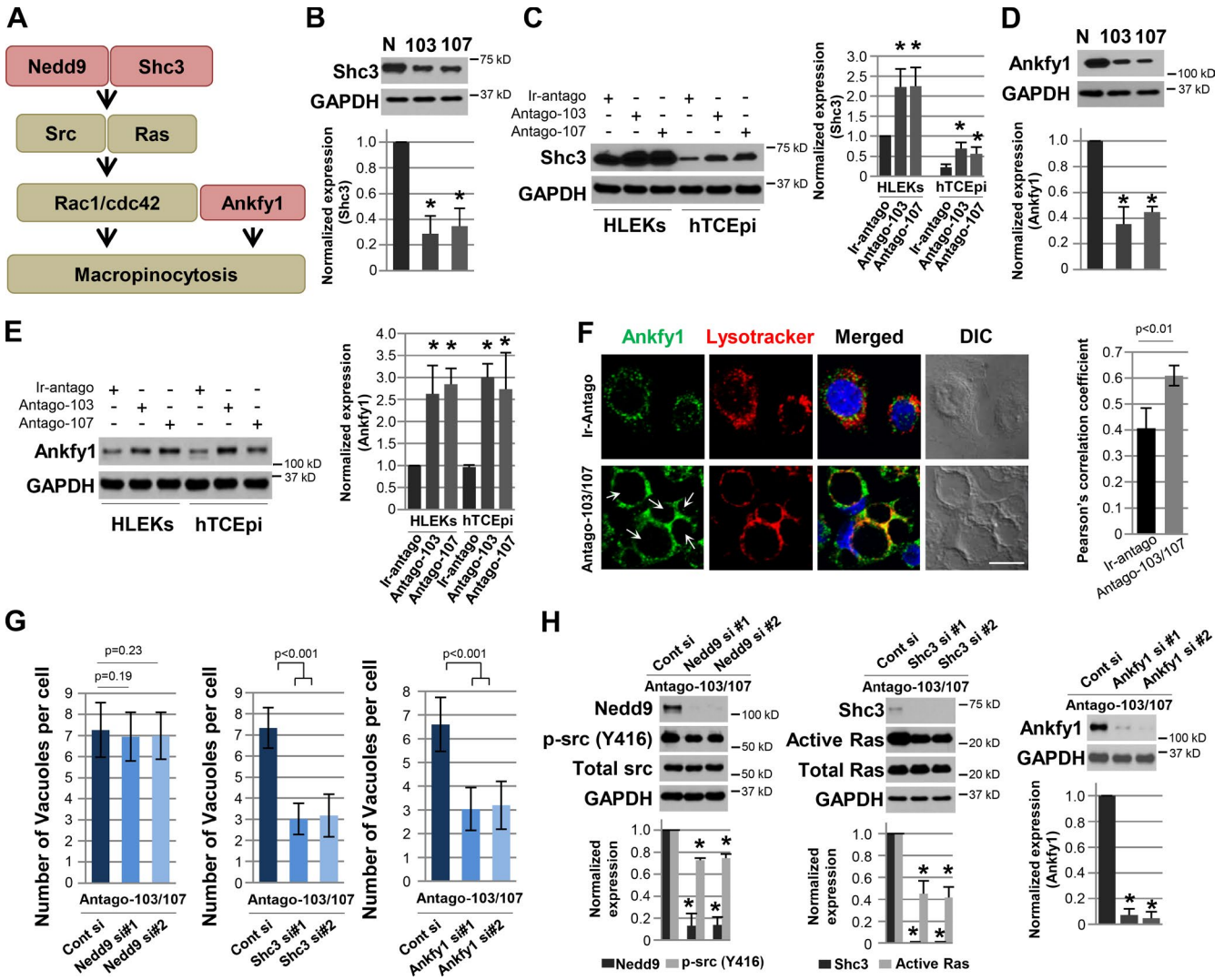

Figure 4. **miR-103/107 target NEDD9, SHC3, and ANKFY1 to regulate aspects of macropinocytosis.** (A) Model of the signaling pathways involved in macropinocytosis that are regulated by miR-103/107. By targeting *NEDD9* and *SHC3*, Src and Ras are partly regulated. Rac1/Cdc42 signaling downstream of active Src and Ras regulates macropinocytosis. Targeting Ankfy1 also contributes to the formation of macropinocytosis. (B) Immunoblotting of endogenous total Shc3 after overexpression of either pre-miR–negative control (N), pre-miR-103 (103), or pre-miR-107 (107) in HLEKs. Normalized expression to GAPDH is included. *, $P < 0.01$. (C) HLEKs and hTCEpi cells were treated with ir-antago, antago-103, or antago-107 for 24 h, and lysates were immunoblotted for Shc3. Normalized expression to GAPDH is included. *, $P < 0.01$. (D) Immunoblotting of Ankfy1 after transfection of pre-miR–negative control (N), pre-miR-103 (103), or pre-miR-107 (107) for 48 h in HLEKs. Normalized expression to GAPDH is included. *, $P < 0.01$. (E) HLEKs and hTCEpi cells were treated with ir-antago, antago-103, or antago-107 for 24 h, and lysates were immunoblotted for total Ankfy1. Normalized expression to GAPDH is included. *, $P < 0.01$. (F) Intracellular localization of Ankfy1 was assessed by confocal microscopy after treatment of HLEKs with either ir-antago or antago-103/107 mixture for 24 h. Arrows indicate representative Ankfy1-stained vacuoles. Pearson's correlation coefficient analysis between LysoTracker Red (DND-99) and Ankfy1 in ir-antago or antago-103/107 HLEKs is shown in the bar graph ($n = 20$ cells for each). Bar, 10 µm. (G and H) The number of vacuoles/cell was determined in Nedd9-, Shc3-, or Ankfy1-depleted HLEKs 48 h after treatment with antago-103/107 mixture (G; $n = 50$ cells), and protein lysates were subjected to immunoblotting (pulldown for active Ras) with antibodies to Nedd9, p-src (Y416), Src, Shc3, Ras, Ankfy1, and GAPDH (H). Normalized levels to GAPDH are included. *, $P < 0.01$. All error bars represent SD.

miR-103/107 maintain dynamin function to ensure lysosome reformation (end-stage autophagy)

The dynamin/AP-2/clathrin machinery is known to play a key role in lysosome reformation as well as lysosome clearance (Powell et al., 2000; Chen and Yu, 2013). Consistent with this idea, AP-2 and clathrin were localized to the vacuoles (Fig. 8 B). Furthermore, after loss of miR-103/107, dynamin 1 was infrequently associated with the cell membrane (Fig. 8 C). This suggests that miR-103/107 may regulate dynamin 1 localization to the membrane and thus affect lysosomal reformation. DAG and its primary target, PKC, regulate many biological processes via phosphorylation of substrates (Krishna and Zhong, 2013). In the context of lysosomal clearance and reformation, dynamin 1, a GTPase enzyme that functions in endocytosis and lysosomal reformation, is regulated by PKC (Fig. 8 A; Powell et al., 2000; Cousin and Robinson, 2001). Using a PKC inhibitor after antago-103/107 treatment for 6 h increased the colocalization of dynamin 1 to the vacuole (Fig. 8 D). Extending treatment for 12 and 24 h markedly reversed the number and size of vacuoles (Fig. 8, E–H). Phosphorylation blocks phospholipid binding by dynamin 1, effectively attenuating endocytosis (Powell et al., 2000) and lysosomal reformation (Chen and Yu, 2013). Antagomir treatment increased (inactivated) phospho-dynamin levels

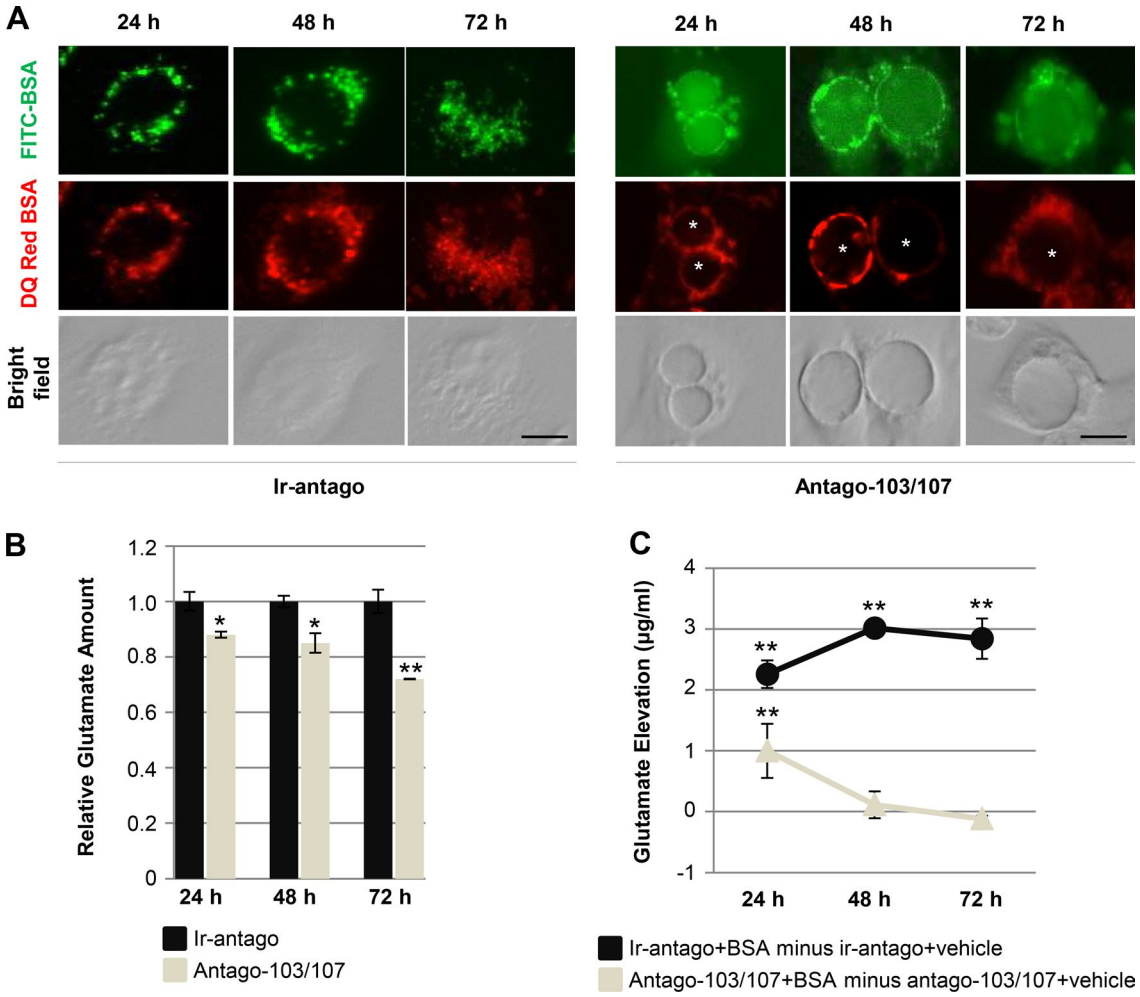

Figure 5. **Vacuoles are defective in digesting protein taken up via macropinocytosis.** (A) Ir-antago or antago-103/107 mixture was simultaneously cotreated in HLEKs with FITC-BSA and DQ-BSA for the indicated times (h). Asterisks indicate no detection of DQ-BSA fluorescence emitted from inside of vacuoles. Bars, 10 µm. (B) HLEKs were treated with ir-antago or antago-103/107 mixture. After treatment for indicated times, cells were lysed and the intracellular level of glutamate was measured and normalized to total protein. The data are expressed as fold change under input control (ir-antago), which was assigned a value of 1. *, $P < 0.01$; **, $P < 0.001$. (C) Intracellular glutamate levels were measured in HLKEs after treatment with either ir-antago or antago-103/107 with and without BSA for indicated times. Elevated amounts of glutamate in the presence of BSA were calculated by subtracting the amount from each corresponding group (ir-antago or antago-107 without BSA). *, $P < 0.01$; **, $P < 0.001$. All error bars represent SD.

(Fig. 8 I). PKC is known to stabilize the cyclin-dependent kinase 5 (CDK5) activator, CDK5R1, a known target of miR-103/107 (Fig. 8 A; Moncini et al., 2011), and CDK5 is a well-known kinase for dynamin (Fig. 8 A; Tomizawa et al., 2003). Antagomir treatment of HLEKs increased CDK5R1 levels (Fig. 8 J), and treatment with roscovitine (12 and 24 h), which inhibits CDK5, resulted in a decrease in the number and size of vacuoles compared with vehicle (Fig. 8, G and H), as well as a decrease in phospho-dynamin levels (Fig. 8 K). Collectively, these observations strongly implicate the involvement of the PKC and CDK5 signaling pathways in dynamin inactivation, which results in vacuole retention (Fig. 8 A). Although we observed a difference in the magnitude of vacuole rescue between these two pathways (Fig. 8 H), both contribute to vacuole formation. To further confirm the roles of CDK5 and PKCα in vacuole formation, we knocked down these two proteins and observed inhibition of vacuole formation (Fig. 8, L and M).

To understand how miR-103/107 regulate the PKC signaling pathway, we identified two targets, *phospholipase D1* (*PLD1*) and *PLD2* (Fig. 9, A and B; and Fig. S5), which are upstream regulators of PKC signaling (Krishna and Zhong, 2013; Fig. 8 A). Using a genetic approach, we showed that knockdown of PLD1 and PLD2 rescued vacuole formation (Fig. 9, C and D). Because PKC can be activated by either PLD or DAG (Krishna and Zhong, 2013), we tested whether PLD (VU0155069) and DAG synthesis inhibitors (D609 and propranolol) would affect antago-103/107–induced vacuole formation. All inhibitors markedly diminished the PKC activity and vacuoles (Fig. 9, E and F), indicating that PLD1 and PLD2 are the main regulators of PKC activity by regulating DAG synthesis. PLD1 and PLD2 are known to regulate PKC via up-regulation of phosphatidic acid (PA) and DAG (Fig. 8 A; Krishna and Zhong, 2013). We reasoned that up-regulation of PA, via a L-α-phosphatidic acid, should reverse the decrease in vacuole formation by PLD and DAG synthesis inhibitors (Fig. 9 G). Indeed, introduction of PA into antago-103/107–treated HLEKs and hTCEpi cells on the background of VU0155069 and D609 dramatically increased the formation of vacuoles (Fig. 9 G), which is strong evidence that miR-103/107 target *PLD1* and *PLD2*, down-regulating PA and DAG synthesis and diminishing PKC activity (Fig. 8 A).

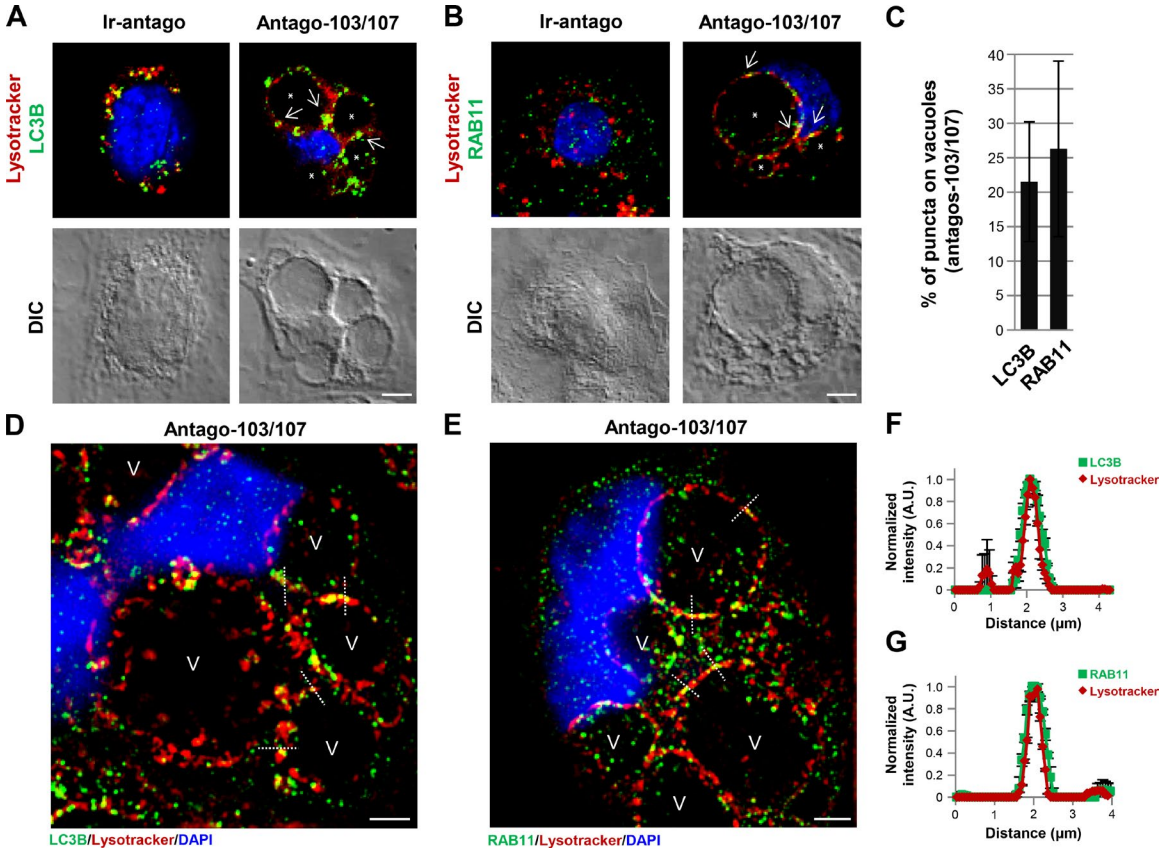

Figure 6. **LC3B and Rab11 are localized in vacuoles.** (A) Representative confocal images of Lysotracker and LC3B staining. HLEKs cells were treated with either ir-antago or antago-103/107 mixture for 24 h. Asterisks indicate vacuoles. LC3B is localized in vacuole membranes (arrows). Bar, 5 µm. (B) HLEKs cells treated with either ir-antago or antago-103/107 mixture for 24 h were subjected to immunofluorescence staining with Lysotracker and Rab11 antibodies. Representative confocal images show the localization of Rab11 in vacuole membranes (arrows). Asterisks indicate vacuoles. Bar, 5 µm. (C) The bar graph shows quantification of LC3B and Rab11 puncta on vacuole membrane in antago-103/107–treated HLEKs (n = 10 cells for each). (D–G) SIM images of LC3B/Lysotracker (D) and Rab11/Lysotracker (E). Line scan analysis (dashed white lines) shows the colocalization of LC3B/Lysotracker (F) and Rab11/Lysotracker (G) on the vacuoles. A.U., arbitrary units; DIC, differential interference contrast; V, vacuoles. Bars, 5 µm. All error bars represent SD.

Such attenuation of PKC activity dephosphorylates (activates) dynamin, enabling proper end-stage autophagy.

Disruption of autophagy affects keratinocyte proliferative capacity

The stem cell–enriched limbal epithelium preferentially expresses miR-103/107, which play important roles in regulating several epithelial stem cell characteristics (Peng et al., 2015) in addition to ensuring proper end-stage autophagy. As a first test of this idea, we argued that because miR-103/107 are limbal epithelial preferred (Peng et al., 2015), this tissue should have increased LC3 staining compared with the corneal epithelium. We took advantage of mice that transgenically express GFP-labeled LC3 (He et al., 2012) and analyzed the limbal and corneal epithelia. Limbal epithelial basal cells had significantly greater amounts of LC3-positive puncta than corneal epithelial basal cells (Fig. 10 A), which is consistent with a role for miR-103/107 in autophagy.

Because the stem cell–enriched limbal epithelia evidenced more active autophagy, we asked whether autophagy would affect keratinocyte proliferative capacity, a hallmark of epithelial stem cells (Potten and Loeffler, 1990; Lavker and Sun, 2000; Blanpain and Fuchs, 2009). The ability of keratinocytes to form holoclone colonies, which are considered to be stem cell derived and represent great growth potential (Barrandon and Green, 1987; Wei et al., 1997; Peng et al., 2015), is an accepted measure of proliferative capacity. We treated HLEKs with either DMSO (vehicle control) or BafA1 (autophagy inhibitor) for 48 h and then assessed viability and the ability to form holoclone colonies. After 48-h treatment with BafA1, HLEKs did not display any difference in apoptosis compared with DMSO treatment (Fig. 10 C) and thus were considered viable. Treated and control HLEKs were seeded at clonal density (200 cells/100-mm dish) and allowed to grow for 2 wk. Colonies were fixed, stained, and analyzed. Interestingly, DMSO-treated keratinocytes formed significantly more holoclone colonies than BafA1-treated cells (Fig. 10 B), indicating that blocking autophagy diminished keratinocyte proliferative capacity. Taking a genetic approach, we knocked down Beclin-1 and Atg7 in HLEKs transduced with empty vector (control) or miR-103 and tested the ability of these cells to form holoclone colonies. We consistently observed a decrease in holoclone colony-forming ability in miR-103–transduced cells deficient in Beclin-1 or Atg7 compared with miR-103–transduced cells, supporting the idea that autophagy plays a positive role in proliferation (Fig. 10 D). To test further this idea, we stressed the corneal epithelium from Beclin-1–deficient mice by making a <1-mm-diameter central corneal epithelial wound and temporally monitored the proliferative status of the reepithelializing tissue for 48 h. There was a significant decrease in the number of cells in S phase ($BrdU^+$

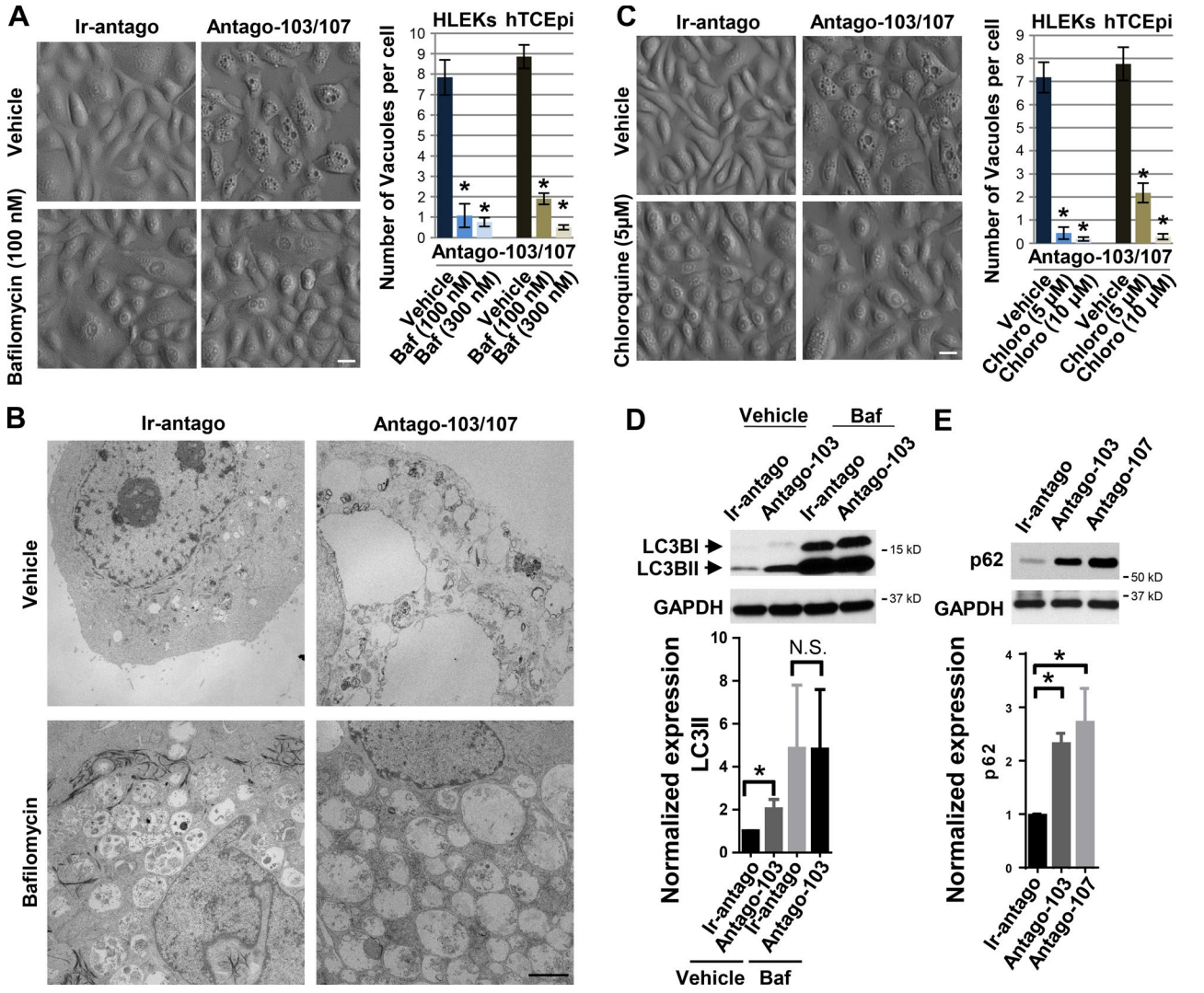

Figure 7. **Vacuole accumulation is caused by a defect in late-stage autophagy.** (A) Representative images of HLEKs simultaneously treated with ir-antago or antago-103/107 mixture with and without BafA1 for 24 h. Bar graph depicts the number of vacuoles/cell in antago-103/107–treated HLEKs and hTCEpi cells with and without BafA1 at indicated concentrations. *n* = 50 cells. *, P < 0.001. Bar, 20 µm. (B) Representative TEM images of HLEKs simultaneously treated with ir-antago or antago-103/107 with and without BafA1. Note the morphologically identical autophagolysosomes in the Baf1-treated cells (arrows). Bar, 2 µm. (C) Representative images of HLEKs simultaneously treated with ir-antago or antago-103/107 mixture with and without chloroquine for 24 h. Quantification of the number of vacuoles/cell (*n* = 50 cells) is shown in the right bar graph. *, P < 0.001. Bar, 20 µm. (D) Cell lysates from HLEKs treated with ir-antago or antago-103 with and without BafA1 (100 nM) were immunoblotted with antibodies against LC3B and GAPDH. *, P < 0.05. (E) Cell lysates from ir-antago or antago-103 HLEKs were immunoblotted with anti-p62. *, P < 0.05. N.S., not statistically significant. All error bars represent SD.

staining) of mitosis during the first 24 h, a time of maximal BrdU labeling after corneal epithelial wounding (Lavker et al., 1998), in the Beclin-1–deficient mouse compared with littermate controls (Fig. 10, E and F). Collectively, these findings indicate that autophagy plays a positive role in proliferation.

Discussion

Here we provide insight into the manner that two important cellular processes, macropinocytosis and autophagy, are coordinately regulated by the miR-103/107 family in a stem cell–enriched epithelium (Fig. 10 G). By targeting *SHC3* and *ANKFY1*, miR-103/107 temper the initiation of macropinocytosis in limbal keratinocytes and prevent the formation of vacuoles (Fig. 10 G). We furnish evidence that under resting conditions, autophagy is greater in the limbal epithelium compared with the corneal epithelium. We show that vacuole accumulation is not a malfunction of the early stages of autophagy; rather, miR-103/107 ensure proper end-stage autophagy by positively regulating dynamin activation necessary for lysosomal reformation (Fig. 10 G). The biological consequence of a disruption in autophagy is a diminution in keratinocyte proliferative capacity, a feature of epithelial stem cells.

miRNAs, macropinocytosis, and autophagy

The vacuoles that form as a result of a loss of miR-103/107 bear a striking resemblance to the extreme cytoplasmic vacuolization seen in cells after hyperstimulation of macropinocytosis or defects in macropinosome recycling (Kitambi et al., 2014; Maltese and Overmeyer, 2015). Furthermore, our finding that miR-103/107 target *NEDD9* and *SHC3*, thereby blocking

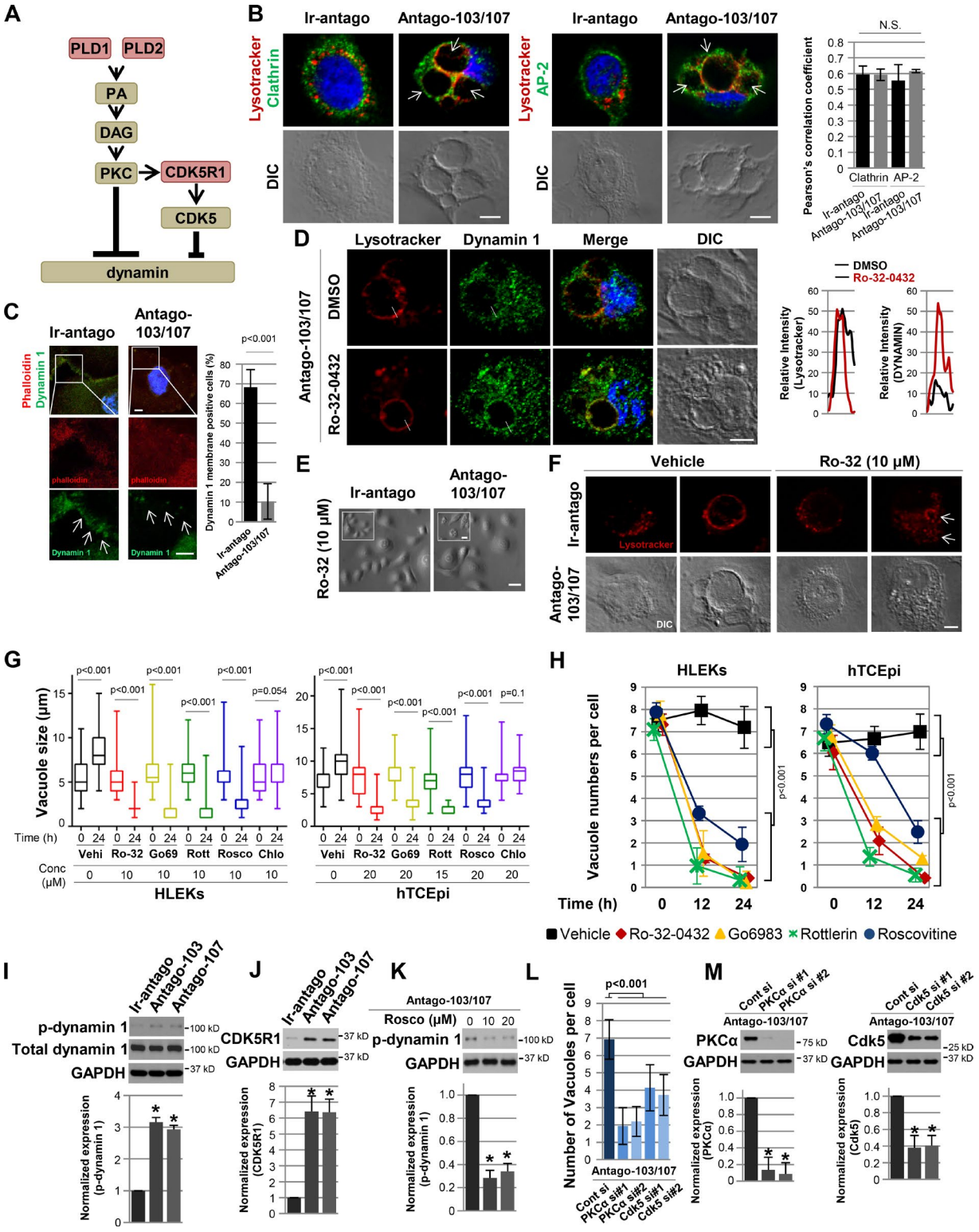

Figure 8. **Vacuole accumulation is due, in part, to dynamin 1 inactivation.** (A) A model of dynamin inactivation by PKC and CDK5 signaling. By targeting *PLD1* and *PLD2*, miR-103/107 regulates DAG synthesis, which activates PKC and inactivates dynamin function. PKC also stabilizes the miR-103/107 target, *CDK5R1*, an activator of CDK5, resulting in the inactivation of dynamin. (B) Representative confocal images showing the localization of clathrin and β-adaptin (AP-2 subunit) to the vacuole membranes. Antago-103/107–treated HLEKs were double stained for clathrin (or β-adaptin, AP-2 subunit) and Lysotracker at 24 h. Arrows indicate vacuoles. The bar graph shows Pearson's correlation coefficient analysis between Lysotracker and clathrin or β-adaptin in ir-antago– or antago-103/107–treated HLEKs (n = 20 cells for each). N.S., not statistically significant. Bars, 5 μm. (C) HLEKs treated with either ir-antago or antago-103/107 mixture for 24 h were stained with a dynamin 1 antibody and phalloidin. Representative confocal images showing less dynamin 1 localization to cell membranes in antago-103/107–treated cells than in ir-antago–treated cells (arrows). The bottom panels show dynamin 1 and phalloidin staining in the indicated subregions. The bar graph shows quantification of dynamin 1 cell membrane–positive cells in ir-antago– or antago-103/107–treated HLEKs (n = 100 cells for each). Bars, 5 μm. (D) HLEKs were treated with antago-103/107 for 24 h to generate vacuoles and

activation of Src, Ras, and ultimately Rac1 signaling, provides new insights into the regulation of this signaling pathway that has been implicated in the triggering of macropinosome-induced vacuolization (Maltese and Overmeyer, 2015). Such defects in macropinocytosis are believed to result in nonapoptotic cell death (Kitambi et al., 2014; Maltese and Overmeyer, 2015). We demonstrate an induction of macropinocytosis by a loss of miRNAs, whereas overexpression of miR-199a-3p in a papillary thyroid carcinoma cell line stimulated macropinocytosis with eventual cell death (Minna et al., 2014). The mechanisms underlying this cell death were not elucidated. Interestingly, cell death was not observed when miR-199a-3p was overexpressed in a nonneoplastic cell line (Minna et al., 2014), consistent with the idea that the function of a given miRNA is context and condition dependent (Jens and Rajewsky, 2015). We did not detect evidence of cell death (e.g., detachment of cells or floating debris, morphologically by TEM analysis, or in viability assays) in HLEKs, hTCEpi cells, or HEKs treated with antagomirs for 72 h. This suggests that, at least in primary cultures of normal keratinocytes, macropinocytosis-induced vacuolization, by itself, is insufficient to trigger cell death, and perhaps tumor cells are more vulnerable to nonapoptotic cell death than normal cells (Maltese and Overmeyer, 2015).

Despite the fact that macropinocytosis was first described in 1931 (Lewis, 1931), it is only in the past decade that advances in the molecular regulation of this process have been achieved (Lim and Gleeson, 2011; Maltese and Overmeyer, 2015). Surprisingly little is known about how miRNAs are involved in this process. In a single study, miR-199a-3p was shown to induce hyperstimulated macropinocytosis when overexpressed in a papillary thyroid carcinoma cell line (Minna et al., 2014). In an in silico analysis of miR-199a-3p, target genes with known gene expression data from an in vitro papillary thyroid carcinoma model indicated that macropinocytosis signaling was one of the predicted pathways (Minna et al., 2014); however, the specific signaling pathways and direct targets regulated by miR-199a-3p–induced macropinocytosis were not elucidated. To our knowledge, the present study represents the first demonstration of how a specific signaling pathway (Src/Ras) and its upstream targets (*NEDD9* and *SHC3*) are regulated by an miRNA family (miR-103/107). Such Src/Ras inhibition can attenuate the initiation of macropinocytosis (vacuoles) in primary epithelial cells. In addition, we are the first to show how miRNAs can regulate the formation of the macropinosome by targeting *ANKFY1*.

Most studies have focused on the early stages of autophagy, because autophagy-related genes function in processes leading to the formation of autophagosomes, and consequently less is known about the late stages of autophagy (Chen and Yu, 2013; Shen and Mizushima, 2014). Autophagic lysosome reformation (ALR) is one of the events that characterize late-stage autophagy (Chen and Yu, 2013). Studies on ALR have been performed on the background of cells under serum and glutamine starvation with mTOR reactivation correlating with the initiation of ALR (Yu et al., 2010; Chen and Yu, 2013; Shen and Mizushima, 2014). We did not observe changes in the mTOR intermediates after antago-103/107 treatment (Fig. S4 B), which suggests that initiation of this process is not compromised. We report that miR-103/107 function in late- or end-stage autophagy by targeting (a) *PLD1* and *PLD2*, which interfere with DAG/PKC signaling; and (b) *CDK5R1,* which regulates CDK5. Such targeting of PLD1/PLD2/DAG/PKC and CDK5R1/CDK5 activates (dephosphorylates) dynamin, which enables vacuole clearance. This suggests the possibility that dysregulation and inactivity of dynamin activators independently regulate vacuole reformation. Consistent with these ideas, clathrin/AP-2 plays a role in ALR (Chen and Yu, 2013), suggesting a commonality between the ALR machinery and the role of miR-103/107 in end-stage autophagy.

Not only do our findings represent one of the first examples of how miRNAs influence the end stage of autophagy (Fig. 8 A), they also suggest that by coordinately regulating aspects of macropinocytosis and autophagy, miR-103/107 link these two processes (Fig. 10 G). The only other connection between autophagy and macropinocytosis was the finding that autophagy-related proteins (LC3, ATG5, ATG7, and a class III phosphatidylinositol (3,4,5)-trisphosphate kinase) can be recruited to both macropinosomes and phagosomes (Florey et al., 2011). However, those authors suggested that macropinocytosis and autophagy are independent.

Macropinocytosis, autophagy, and the limbal epithelium

Our findings raise several interesting questions. First, why would the limbal (stem cell–enriched) epithelium need to attenuate macropinocytosis and not the adjacent corneal epithelium? The limbal epithelium is subtended by a loosely organized, highly vascularized, stroma (Wei et al., 1993), thus affording it ready access to nutrients. Conversely, the corneal epithelium rests on a highly organized, tightly packed, avascular, stroma (Wei et al., 1993) with limited access to nutrients. Because macropinocytosis is a means for cells to nonselectively ingest large amounts of extracellular fluid and nutrients (Lim and Gleeson, 2011), the highly vascularized limbal stroma may negate the need for macropinocytosis, whereas this process might play a role in the corneal epithelium under normal and pathological

exposed to the PKC inhibitor (Ro-32-0432) for another 6 h. Representative confocal images and a graph of the Lysotracker or dynamin 1 intensity profiles using ImageJ software indicate that PKC inhibition results in more dynamin 1 localization in vacuoles. Bar, 5 µm. (E) Representative phase-contrast micrographs of HLEKs sequentially treated with ir-antago or antago-103/107 and Ro-32-0432. HLEKs were treated with either ir-antago or antago-103/107 mixture for 24 h and exposed to the PKC inhibitor (Ro-32-0432) for another 24 h. Insets are images of HLEKs treated with vehicle (DMSO) after treatment with either ir-antago or antago-103/107. Bars, 20 µm. (F) HLEKs were treated with antago-103/107 for 24 h to generate vacuoles and exposed to the PKC inhibitor (Ro-32-0432) for another 6 h. Representative confocal images show vacuoles undergoing disruption (arrows). Bar, 5 µm. (G and H) HLEKs were treated with antago-103/107 for 24 h to generate vacuoles and exposed to the PKC (Ro-32-0432, Go6983, and Rottlerin) and cdk5 (roscovitine) inhibitors and chloroquine for 12 or 24 h. The size (G) and number (H) of vacuoles are presented in the bar graphs. (I) Cell lysates from ir-antago–, antago-103–, or antago-107–treated HLEKs were immunoblotted with antibodies against p-dynamin 1, dynamin 1, and GAPDH. *, $P < 0.01$. (J) Cell lysates from ir-antago–, antago-103–, or antago-107–treated HLEKs were immunoblotted with antibodies against CDK5R1 and GAPDH. *, $P < 0.01$. (K) Cell lysates from antago-103/107–treated HLEKs with roscovitine at different concentrations were immunoblotted with antibodies against p-dynamin 1 and GAPDH. *, $P < 0.01$. (L and M) The number of vacuoles/cell was determined in PKCα- or CDK5-depleted HLEKs 48 h after treatment with antago-103/107 mixture (L; $n = 50$ cells), and protein lysates were subjected to immunoblotting with antibodies to PKCα, CDK5, and GAPDH (M). Normalized levels to GAPDH are included. DIC, differential interference contrast. *, $P < 0.01$. All error bars represent SD.

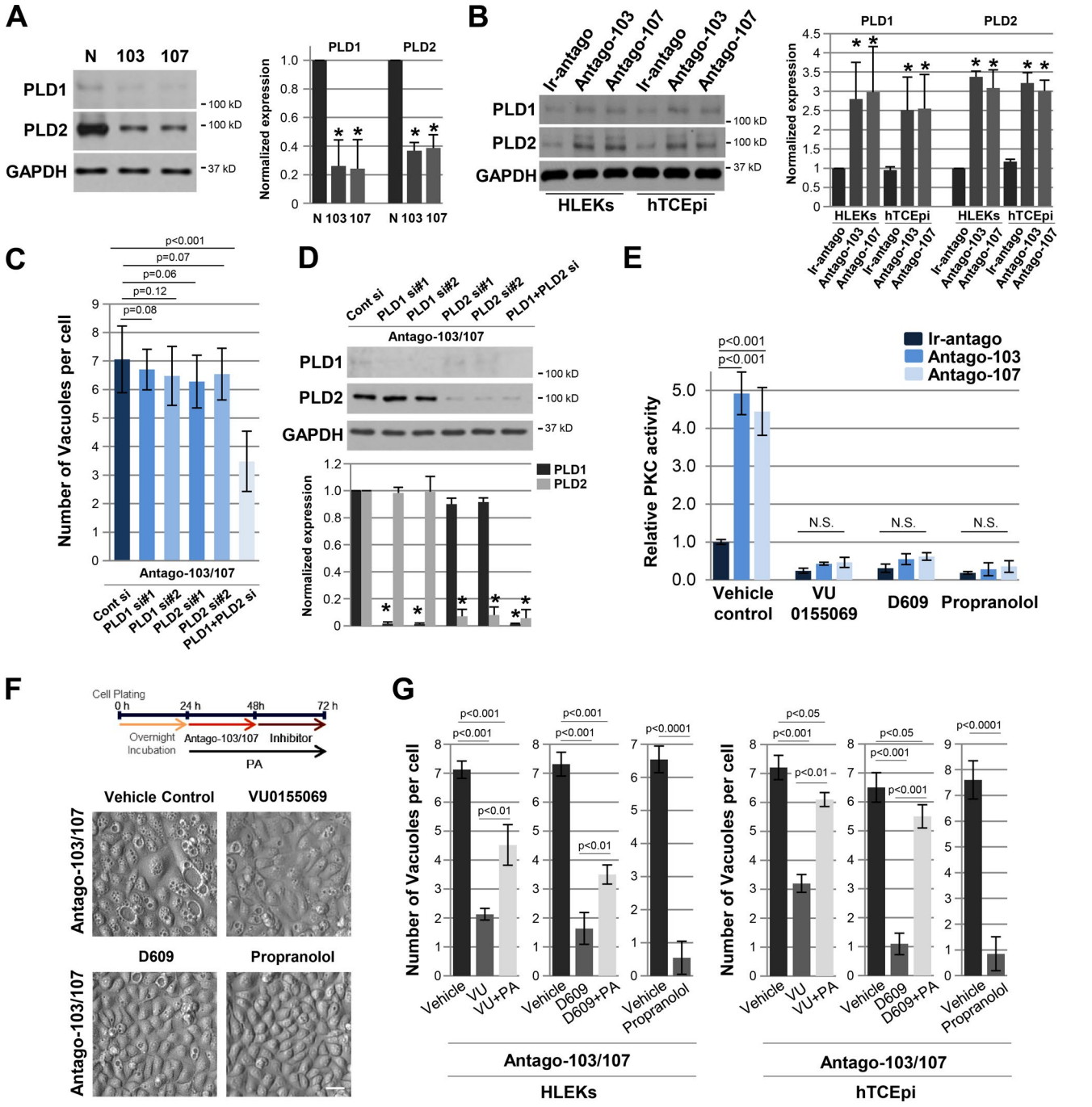

Figure 9. **miR-103/107 modulate DAG synthesis to minimize vacuole accumulation.** (A) Immunoblotting of PLD1 and PLD2 after overexpression of pre-miR–negative control (N), pre-miR-103 (103), or pre-miR-107 (107) in HLEKs. Normalized expression to GAPDH is included. *, $P < 0.01$. (B) HLEKs and hTCEpi cells were treated with ir-antago, antago-103, or antago-107 for 24 h, and lysates were immunoblotted for PLD1 and PLD2. Normalized expression to GAPDH is included. *, $P < 0.01$. (C and D) The number of vacuoles/cell was determined in PLD1- and PLD2-depleted HLEKs 48 h after treatment with antago-103/107 mixture (C; $n = 50$ cells), and protein lysates were subjected to immunoblotting with antibodies to PLD1, PLD2, and GAPDH (D). Normalized levels to GAPDH are included. *, $P < 0.01$. (E) HLEKs cells simultaneously treated with ir-antago, antago-103, or antago-107 with and without a pharmacological inhibitor of PLD (VU0155069; 10 μM) and DAG synthesis inhibitors (D609 at 100 μM and propranolol at 100 μM) for 24 h. Active PKC was examined using PKC substrate microtiter plates. The data are expressed as fold change under input control (ir-antago + vehicle), which was assigned a value of 1. (F) Representative phase-contrast microscope images of hTCEpi cells treated with VU0155069 (10 μM), D609 (100 μM), and propranolol (100 μM) followed by treatment with antago-103/107 mixture. Bar, 20 μm. (G) Quantification of the number of vacuoles/cell is presented in the bar graphs. HLEKs and hTCEpi cells were treated with antago-103/107 mixture for 24 h, and cells were exposed to VU0155069 (10 μM), D609 (100 μM), and propranolol (100 μM) for another 24 h. To compensate for the loss of PA after treatment of either VU0155069 or D609, L-α-phosphatidic acid (300 μM) was pretreated along with antago-103/107 mixture. N.S., not statistically significant. All error bars represent SD.

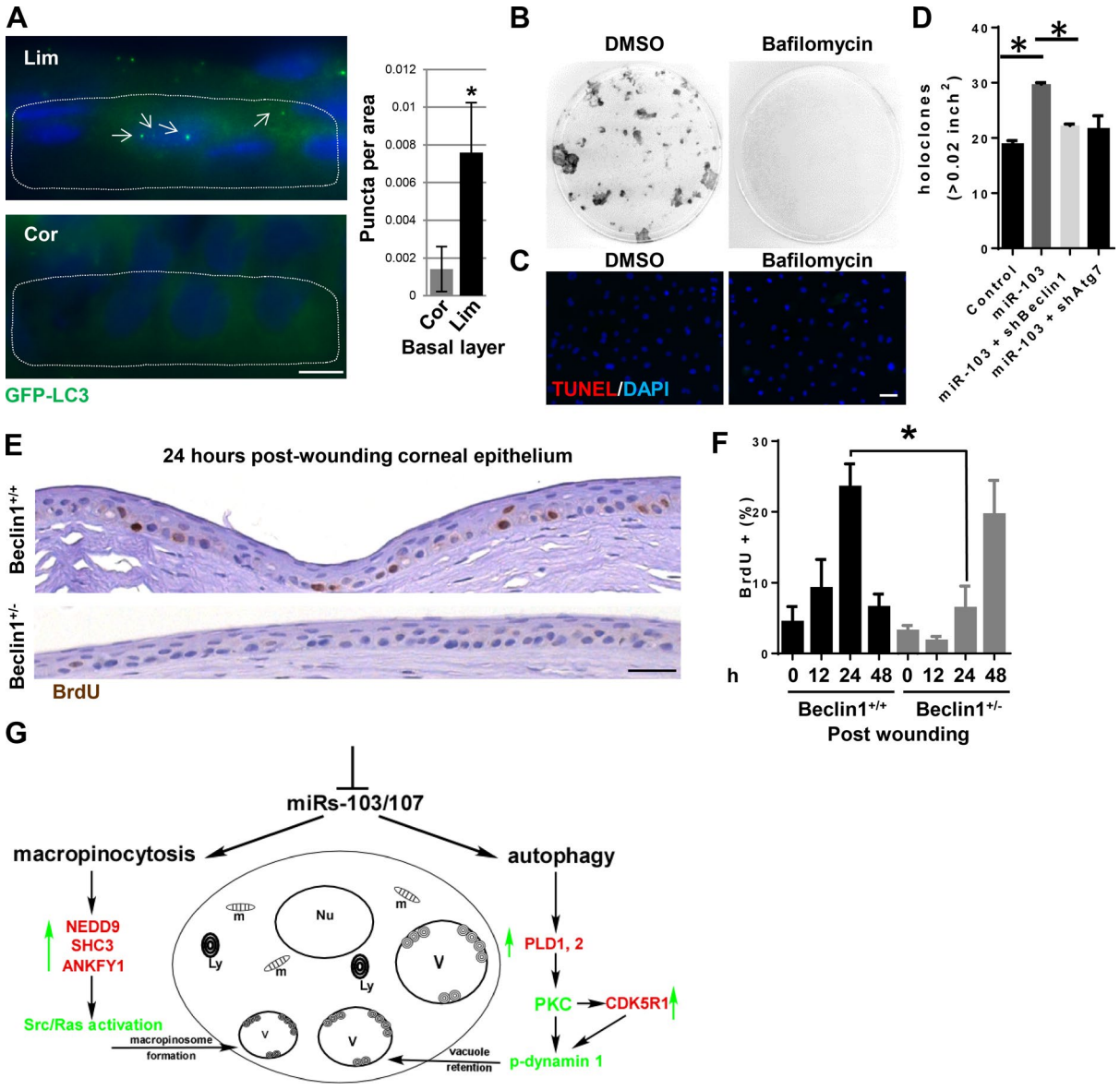

Figure 10. **Inhibition of autophagy negatively affects epithelial proliferative capacity.** (A) Representative frozen sections of portions of the limbal (Lim) and corneal (Cor) epithelia from GFP-LC3 transgenic mice showing puncta (autophagosomes) localized primarily in limbal basal cells (arrows). Dotted lines outline the limbal and corneal basal layers. Quantification of the distribution of puncta is presented in the bar graphs. Bar, 2 µm. (B) Holoclone-forming assay of HLEKs as a function of treatment with BafA1. BafA1-treated keratinocytes gave rise to significantly fewer holoclones than the vehicle (DMSO) control. 200 cells per plate were seeded for each treatment. (C) After the same treatment conditions, HLEKs cells were subjected to TUNEL and counterstained with DAPI. Bar, 20 µm. (D) Holoclone-forming assay in keratinocytes transduced with shBeclin-1 or shATG7 in the presence of miR-103 overexpression. Cells after transduction of pCDH or miR-103 lentiviral constructs were transduced with shRNA targeting Beclin-1 or ATG7. shBeclin-1 or shATG7 + miR-103–transduced keratinocytes gave rise to significantly fewer holoclones than miR-103–transduced cells alone. 200 cells per plate were seeded for each treatment. $n = 3$; *, $P < 0.05$. (E and F) Central corneal epithelia of mice with allelic loss of the autophagy gene *Beclin-1* (*Beclin-1*$^{+/-}$), which have decreased Beclin-1 protein expression and autophagy, were removed by application of a rotating diamond burr to the surface of the central cornea. Immunohistochemical analysis of BrdU in epithelia was conducted. Representative images 24 h after wounding epithelia were acquired (E), and the percentage of BrdU-labeled cells was counted (F). Note that BrdU labeling in *Beclin-1*$^{+/+}$ mouse corneal epithelium showed a maximum increase at 24 h after wounding, whereas BrdU labeling in *Beclin-1*$^{+/-}$ was not induced at 24 h after wounding. $n = 3$; *, $P < 0.05$. Bar, 10 µm. (G) Schematic representation of how miR-103/107 coordinately regulate aspects of both macropinocytosis and autophagy. Loss of miR-103/107 has two effects: (a) Such loss up-regulates macropinocytosis via targeting *NEDD9*, *SHC3*, and *ANKFY1*, which collectively activates Src/Ras. This yields numerous vacuoles. (b) Such loss up-regulates PLD1 and PLD2, as well as CDK5R1, which inactivates dynamin 1, causing vacuole retention. Red, direct targets of miR-103/107; green, key factors; green arrows, up-regulation; Ly, lysosomes; m, mitochondria; Nu, nucleus; V, vacuoles. All error bars represent SD.

circumstances. Additionally, the limbal epithelial basal layer is populated with stem cells (Schermer et al., 1986; Cotsarelis et al., 1989; Stepp and Zieske, 2005; Sun et al., 2010), which, by definition, are relatively quiescent (Potten and Loeffler, 1990), minimizing the need for large infusions of solutes and nutrients via macropinocytosis.

Second, why does the limbal basal epithelium have more autophagy than the corneal basal epithelium? This most likely reflects the aforementioned fact that the corneal epithelial stem cells are preferentially located in the limbal epithelium (Schermer et al., 1986; Cotsarelis et al., 1989). Our finding of significantly more LC3 puncta in the resting limbal basal (stem

cell–enriched) cells compared with corneal epithelial basal cells is indicative that autophagy is up-regulated in this tissue. This is consistent with studies in other tissues (e.g., human bone marrow mesenchymal stem cells, rat oocytes immediately after fertilization by spermatozoa, and mouse bone marrow stromal cells differentiating into osteoblasts) of a high level of constitutive autophagy that decreases in more differentiated cells (Oliver et al., 2012; Guan et al., 2013). Unlimited self-renewal, quiescence, and differentiation into TA cells are hallmarks of stem cells (Potten and Loeffler, 1990). There is increasing evidence that activation of autophagy is required for these processes to properly function. For example, hematopoietic stem cells (HSCs) lacking certain autophagic genes are incapable of serial transplantation into compromised recipient mice, indicating that autophagy is required for self-renewal (Mortensen et al., 2011). We demonstrate that blocking autophagy in HLEKs markedly diminishes the ability of these cells to form holoclone (stem cell–derived) colonies (Fig. 10), suggesting that autophagy may function to maintain proliferative capacity. Furthermore, we show that in autophagy-deficient (*Beclin-1*$^{+/-}$) mouse cornea, there is a significant delay in proliferation after wounding. This delay may be caused by a failure in limbal stem/progenitor cell activation. Consistent with this idea, HSCs lacking Atg7 display a marked loss of colony-forming ability (Mortensen et al., 2011). More recently, it has been shown that autophagy is induced in activated muscle stem or satellite cells, and that inhibition of autophagy blocks activation (e.g., BrdU incorporation) in these cells (Tang and Rando, 2014). Although autophagy is frequently associated with a decrease in proliferation (Ramírez-Valle et al., 2008; Wu et al., 2008; Chen et al., 2013; Cianfanelli et al., 2015), several studies have shown that proliferation is enhanced or maintained by autophagy (Bell et al., 2008; Liu et al., 2014; Tang and Rando, 2014; Yazdankhah et al., 2014). With respect to cell fate commitment or differentiation, in HSCs, mesenchymal stem cells, and neuronal stem cells, as well as HaCat cells, autophagy is generally believed to play a positive role (Aymard et al., 2011; Vessoni et al., 2012; Guan et al., 2013; Phadwal et al., 2013).

The preferential expression of the miR-103/107 family in the stem cell–enriched limbal epithelium makes perfect biological sense, as this family contributes to proper end-stage autophagy, a process essential for stem cell maintenance. Given the positive regulatory effects that this miRNA family has on other epithelial stem cell characteristics (e.g., cell proliferation, proliferative capacity, and cell–cell communication; Peng et al., 2015), the present work reinforces the idea that miR-103/107 are vital for homeostasis of epithelial stem cells.

Materials and methods

Cell culture, antagomir treatment, and transfection

Corneas were provided by Eversight. As previously described (Peng et al., 2015), primary HLEKs were isolated from cadaver donor corneas and cultured in CnT-20 medium with supplements (CELLnTECH) using collagen IV–coated plates (BD). hTCEpi, which is the limbal-derived epithelial cell line, was cultured in Keratinocyte SFM medium (Invitrogen) at 0.15 mM $CaCl_2$. Cells were transfected with 50 nM miRNA mimics specifying miR-103 and miR-107 and nontarget control (GE Healthcare) as previously described (Yu et al., 2008). For lentiviral transduction, cells were incubated within lentiviral supernatants (produced by the Northwestern University Skin Disease Research Center RNA/DNA Delivery Core Facility) for 6 h and then switched to fresh growth medium. For siRNA transfection, cells were transfected with 50 nM siRNA against Rac1, Cdc42, Src, Kras, Nedd9, Shc3, Ankfy1, PKCα, Cdk5, PLD1, PLD2, and nontarget control (GE Healthcare) as previously described (Yu et al., 2008). ON-TARGETplus SMARTpool (GE Healthcare) was used for Rac1 and Cdc42. The target sequences of other siRNAs were as follows: Src #1, 5′-CCA AGGGCCUCAACGUGAA-3′; Src #2, 5′-GGGAGAACCUCUAGG CACA-3′; Kras #1, 5′-GGAGGGCUUUCUUUGUGUA-3′; Kras #2, 5′-GAAGUUAUGGAAUUCCUUU-3′; Nedd9 #1, 5′-CCUCUGGAC UGAUGCAGCA-3′; Nedd9 #2, 5′-CCAAGAACAAGAGGUAUAU-3′; Shc3 #1, 5′-GAACACAAAUUACCAGGGA-3′; Shc3 #2, 5′-GAA GUUCUGCGCUCAAUGA-3′; Ankfy1 #1, 5′-GGUGUUAUGUCU CUAGUGA-3′; Ankfy1 #2, 5′-GUGCAAACAACUAGAUUUA-3′; PKCα #1, 5′-UAAGGAACCACAAGCAGUA-3′; PKCα #2, 5′-GAA GGGUUCUCGUAUGUCA-3′; Cdk5 #1, 5′-UAUAAGCCCUAUCCG AUGU-3′; Cdk5 #2, 5′-GGAUUCCCGUCCGCUGUUA-3′; PLD1 #1, 5′-CAACAGAGUUUCUUGAUAU-3′; PLD1 #2, 5′-GGUAAUCAG UGGAUAAAUU-3′; PLD2 #1, 5′-GGACCGGCCUUUCGAAGAU-3′; and PLD2 #2, 5′-CAGCAUGGCGGGACUAUAU-3′. For antagomir treatment, HLEKs and hTCEpi cells were treated with 1,500 pg/ml of the following antagomirs from GE Healthcare: antago-103, mU(*) mC(*)mA(*)mUmAmGmCmCmCmUmGmUmAmCmAmAmUmG-mCmU(*)mG(*)mC(*)mU - Chol; antago-107, mU(*)mG(*)mA(*)mU mAmGmCmCmCmUmGmUmAmCmAmAmUmGmCmU(*)mG(*) mC(*)mU-Chol; and ir-antago, mG(*)mG(*)mC(*)mAmUmUmC-mAmCmCmGmCmGmUmGmCmC(*)mU(*)mU(*)mA-Chol; where mN means 2'-*O*-methyl–modified oligonucleotide, (*) means a phosphorothioate linkage, and Chol means linked cholesterol.

Inhibitors

Pharmacological inhibitors used in this study are summarized in Fig. S1 and Table S1. HLEKs or hTCEpi cells were plated in a six-well plate. After overnight incubation, the cells were exposed to ir-antago, antago-103, or antago-107 (or mixture of antago-103 and antago-107) with and without an inhibitor. For the sequential treatment schedule, cells were treated with ir-antago, antago-103, or antago-107 for 24 h for the generation of vacuoles. After 24 h, each inhibitor was applied in cells. Amiloride, EIPA, roscovitine, manumycin A, Ro-32-0432, FAK inhibitor 14, NSC23766, EUK134, 8-bromo-cAMP, VU0155069, Go6983, Rottlerin, IBMX, and propranolol hydrochloride were obtained from Santa Cruz Biotechnology, Inc.; *O*-tricyclo[5.2.1.0(2,6)] dec-9-yl dithiocarbonate potassium salt (D609), L-α-phosphatidic acid sodium salt, and chloroquine were obtained from Sigma-Aldrich. BafA1 was from Cayman. PP2 was from EMD Millipore. ZCL278 was from Tocris Bioscience. SB203580 was from Cell Signaling Technology. BI-D1870 was from Enzo Life Sciences. Z-VAD-FMK was from BD. For short-term treatment of BafA1, cells were pretreated with BafA1 for 1 h, then medium with BafA1 was removed and cells were incubated in fresh medium with antagomirs for 24 h.

Mice

Eyes of GFP-LC3 transgenic mice, which systemically express GFP fused to LC3 (Mizushima et al., 2004), were rapidly dissected out and embedded in optimal cutting temperature compound rapidly. 5-µm frozen sections were fixed in 4% PFA at RT for 10 min. After three washes with PBS, the sections were mounted using HardSet Antifade Mounting Medium with DAPI (VectaShield). Images were taken using a 100× objective in an epifluorescence microscope AxioVision Z1 (ZEISS). DAPI was used to counterstain nuclei, and GFP punctas were counted. The *Beclin-1*$^{+/-}$ mouse has been described (Qu et al., 2003). Central corneal epithelia of *Beclin-1*$^{+/-}$ and *Beclin-1*$^{+/+}$ mice were removed by

application of a rotating diamond burr to the surface of the central cornea. The limbal epithelium remained intact. Tissues were embedded in paraffin blocks for immunohistochemical analysis of BrdU. Animal procedures were approved by the Northwestern University Animal Care and Use Committee.

Transmission electron microscopy

For TEM, cells were fixed in 2% paraformaldehyde and 2.5% glutaraldehyde in 0.1 M sodium cacodylate buffer and processed for thin sectioning as previously described (Lavker, 1979). Ultrathin sections were made with a Microtome UCT (Leica Biosystems), and grids were viewed with a FEI Tecnai Spirit G2 transmission electron microscope at 120 kV. The number of vacuoles was counted under bright-field light microscopy, and the size of vacuoles was measured in randomly selected bright-field images using ImageJ.

Immunostaining and immunohistochemistry

Cells were fixed with 4% PFA at RT for 10 min. Slides were incubated overnight with antibodies against LAMP1, EEA1, AP-2 (1:100; Santa Cruz Biotechnology, Inc.), LC3B, Rab11, clathrin, and dynamin 1 (1:100; Cell Signaling Technology). After washing, slides were incubated with Alexa Fluor–linked secondary IgG (Vector Laboratories). DAPI was used to counterstain nuclei (Peng et al., 2012, 2015). For illustrating lysosomes and their pH, cells were incubated with 75 nM LysoTracker red DND-99 (Invitrogen) for 20 min before being fixed with 4% PFA for 10 min. To examine filamentous actin, coverslips were incubated for 2 h at RT with rhodamine-conjugated phalloidin (1:50; Sigma-Aldrich). For Lucifer Yellow uptake, HLEKs and hTCEpi cells were treated with ir-antago or antago-103/107 mixtures, incubated with warm medium containing 200 µg/ml Lucifer Yellow (Thermo Fisher Scientific) for 4 h, and washed three times with Dulbecco's PBS. For BrdU immunohistochemistry to detect proliferation, antigen retrieval of the paraffin sections was performed at 70°C in formamide retrieval solution (1× SCC in formamide) for 1 h. After blocking in PBS containing 0.01% BSA and 0.01% Tween-20, sections were incubated for 30 min with BrdU monoclonal antibody (1:10; Developmental Studies Hybridoma Bank). Sections were incubated with the corresponding biotinylated secondary antibody (1:200; Vector Laboratories) and then with HRP–streptavidin conjugate (Invitrogen). Signal was detected using the Zymed DAB Plus Substrate kit according to the manufacturer's instructions. Sections were counterstained with hematoxylin to visualize morphology and mounted in Permount. TUNEL assay (In Situ Cell Death Detection kit; Roche) was conducted on the slides according to the manufacturer's instructions by image analysis using AxioVision software (ZEISS). DAPI was used to counterstain nuclei.

BSA uptake and glutamate assay

HLEKs were treated with either ir-antago or antago-103/107 in the presence of FITC-BSA (10 µg/ml; Sigma-Aldrich) and DQ-Red-BSA (10 µg/ml; Thermo Fisher Scientific). For the glutamate assay, HLEKs were treated with either ir-antago or antago-103/107 in the presence or absence of BSA (100 µg/ml; Sigma-Aldrich), lysates were extracted at each time point, and glutamate levels were measured using a colorimetric glutamate assay kit (Sigma-Aldrich) according to the manufacturer's instructions.

Microscope image acquisition

Phase-contrast images were taken using an AxioCam MR digital camera mounted on an Axiovert 40CFL inverted light microscope (ZEISS). The number of vacuoles per cell was counted under LD 20×/0.30 PH1 Var 1 (ZEISS) at RT. AxioVision software (ZEISS) was used to acquire the images. The size of vacuoles was measured in randomly selected bright-field images using ImageJ. For immunohistochemistry, images were obtained using an AxioCam HR digital camera mounted on an Axioplan 2 bright-field microscope system with a Plan-Neofluar 40×/0.75 objective (ZEISS) at RT. AxioVision software was used to acquire and analyze the images. Fluorescent images were acquired using EC Plan-Neofluar 20×/0.5, EC Plan-Neofluar 40×/0.5, and Plan Apochromat 100×/1.4 Oil Ph.3 objectives on an epifluorescence microscope system (AxioVision Z1; ZEISS) fitted with a slide module (Apotome; ZEISS) and a digital camera (AxioCam MRm; ZEISS) at RT. AxioVision software was used to acquire and analyze the images. Alexa Fluor 555 and 488 were used. For confocal microscopy, images were acquired using a laser-scanning confocal microscope imaging system (UV LSM 510 META; ZEISS) with a Plan Apochromat 63 chroma/1.4 oil-immersion objective at RT. LSM software (ZEISS) was used to acquire and analyze the images. Alexa Fluor 555 and 488 were used.

For superresolution microscopy, cells were imaged with SIM (N-SIM; Nikon) equipped with multiple colors (405, 488, and 561) with an EM-CCD camera iXon3 DU-897E (Andor Technology) and a 100× apo 1.49-NA objective lens at RT. Image acquisition was performed with the 3D SIM mode, and image reconstruction was performed with the Nikon NIS Elements software package. Alexa Fluor 555 and 488 were used. Western blot and colony formation assay images were acquired with a desktop image scanner (Epson) at RT.

PKC activity assay

HLEKs were treated with ir-antago, antago-103, or antago-107 with and without an inhibitor (VU0155069, D609, and propranolol). After 24-h treatment, cells were lysed, and the level of PKC kinase activity was measured using a PKC kinase activity assay kit (Abcam) according to the manufacturer's instructions. Assays were performed in triplicate; mean ± SD is shown.

Western blotting

We extracted cells with RIPA cell lysis buffer (50 mM Tris-HCl, pH 7.4, 150 mM NaCl, 0.25% deoxycholic acid, 1% NP-40, 1 mM EDTA, 1 mM phenylmethylsulfonyl fluoride, phosphatase inhibitor cocktail [Thermo Fisher Scientific], and protease inhibitor cocktail [Thermo Fisher Scientific]). 4–20% Tris-HCl gradient gels (Bio-Rad Laboratories) were used to separate proteins. After transferring to PVDF membranes, blots were blocked in 5% nonfat milk in TBS/Tween 20 and incubated with antibodies overnight at 4°C (Peng et al., 2012). Blots were washed with TBS/Tween 20 and incubated with secondary antibodies conjugated with HRP for 1 h at RT. SuperSignal West Dura extended-duration substrate (Thermo Fisher Scientific) was used for detecting HRP on immunoblots. The following antibodies raised in rabbit were used: PKCα, CDK5, Rac1/Cdc42, Nedd9, p-src (Y416), p-src (Y527), src, p-mTOR (S2448), p-mTOR (S2481), mTOR, Raptor, p-Raptor, GβL, DEPTOR, LC3B, Atg3, Atg5, Atg7, Beclin-1, PLD1, PLD2, p35, dynamin 1 (Cell Signaling Technology), and GAPDH (Santa Cruz Biotechnology, Inc.). The following antibodies raised in mouse were used: Ras, Ankfy1, SHC3, and p62 (Santa Cruz Biotechnology, Inc.). The following antibody raised in goat was used: p-dynamin 1 (Santa Cruz Biotechnology, Inc.). Pull-down assays of ras, rac1, and cdc42 were performed according to the suppliers' instructions using active ras, rac1, and cdc42 detection kits (Cell Signaling Technology).

Luciferase reporter assay

The 3′ UTRs of targets, which were predicted by TargetScan, were amplified by PCR using human genomic DNA as a template and a LongAmp Taq DNA Polymerase (New England BioLabs, Inc.). PCR products were digested with XhoI (or AsiSI) and NotI, gel purified,

and ligated into the psiCHECK-2 vector (Promega). Primer sequences used in this study were designed by Integrated DNA Technologies. Primer sequences were as follows: SHC3, sense 5′-ATATGCGAT CGCACCTGGAGTGGACTAGAAT-3′ and antisense 5′-ATTAGC GGCCGCTACTTTTCACAACAGCCTTTATTGC-3′; ANKFY1, sense 5′-CTGCCTCGAGTCGTCACTGCGGACGTCTTC-3′ and antisense 5′-ATTAGCGGCCGCGTAGGCACTTAAGTTTATGGG AAATTTC-3′; PLD1, sense 5′-CTGCCTCGAGGAGATATTCAT TGGCAGCTCA-3′ and antisense 5′-ATTAGCGGCCGCTTTTCA TTTCATTAGCTCTCTCCTT-3′; and PLD2, sense 5′-CTGCCTCGA GTAGCAAGGAGGGCATGAT-3′ and antisense 5′-ATTAGCGGC CGCAACCTTTTCTACACCTTTATTTATGAAATG-3′. Luciferase reporter assays were conducted as described previously (Peng et al., 2012, 2015). Constructs were cotransfected with miR-control (negative control), miR-103, or miR-107 into cells using siRNA transfection reagent (RNAiMAX; Invitrogen). 24 h after transfection, cell lysates were used to measure both firefly and renilla luciferase activities using the Dual-Luciferase Reporter Assay System (Promega) according to the manufacturer's instructions.

Colony formation assay

1,000 HLEKs were seeded in a 100-mm plate and cultured with mitomycin C–treated 3T3 feeder cells in FAD medium (DMEM/F12, 10% FCS, 5 µg/ml insulin, 0.18 mM adenine, 0.4 µg/ml hydrocortisone, 10 ng/ml cholera toxin, 5 µg/ml triiodothyronine, 5 µg/ml human apotransferrin, 4 mM glutamine, 50 IU/ml penicillin-streptomycin, and 10 ng/ml epidermal growth factor; Peng et al., 2015). To test whether inhibition of autophagy can affect colony formation, keratinocytes were pretreated with 100 nM BafA1 or DMSO for 3 d. To test whether autophagy is required for increased holoclone colony formation, the cells with miR-103 overexpression were lentivirally transduced with shRNAs targeting Beclin-1 and Atg7 for 3 d. Then cells were plated and incubated in FAD medium for 2 wk at 200 cells per plate. Colonies were visualized by staining with methanol/crystal violet. Colony size was measured using ImageJ.

Real-time quantitative PCR

HLEKs were treated with antago-103, antago-107, and ir-antago, and total cellular RNA was isolated and purified with an mRNeasy kit (QIAGEN). TaqMan miRNA assay (Applied Biosystems) was performed according to the manufacturer's instructions. Real-time quantitative PCR was performed on a Roche LightCycler 96 System using the Roche FastStart Essential DNA Green Master according to the manufacturer's instructions.

Statistical analysis

Unpaired *t* test and analysis of variance were used to determine statistical significance. The data are shown as means ± SD. The differences were considered significant for p-values of <0.05. All experiments were replicated at least three times.

Online supplemental material

Fig. S1 shows antagomir specificity, TEM images of vacuoles, and pharmacological inhibitor screening in vacuole formation. Fig. S2 shows that miR-103/107 regulate macropinocytosis via targeting of *SHC3*/Ras and *Ankfy1*. Fig. S3 shows that inhibition of autophagy induction rescues vacuole accumulation in antago-103/107–treated HLEKs. Fig. S4 shows that miR-103/107 regulate autophagy independent of the mTOR pathway and genes that relate to induction of autophagy. Fig. S5 demonstrates that *PLD1* and *PLD2* are bona fide targets of miR-103/107. Table S1 summarizes the pharmacological inhibitors used in this study.

Acknowledgments

Lentiviral constructs were obtained from the Northwestern University Skin Disease Research Center (NU-SDRC) DNA/RNA Delivery Core Facility and the NU-SDRC Morphology and Phenotyping Core Facility assisted in morphological analysis.

The NU-SDRC is supported by the National Institute of Arthritis and Musculoskeletal and Skin Diseases grant AR057216. This research is supported by National Institutes of Health grants EY06769, EY017539, and EY019463 (to R.M. Lavker) and DK094980 (to C.C. He); National Natural Science Foundation of China grant 31300814 (to Y. Dong); a Dermatology Foundation research grant and Career Development Award (to H. Peng); and a MidWest Eye Bank research grant (to H. Peng).

The authors declare no competing financial interests.

Submitted: 8 April 2016
Revised: 29 August 2016
Accepted: 1 November 2016

References

Araki, N., M.T. Johnson, and J.A. Swanson. 1996. A role for phosphoinositide 3-kinase in the completion of macropinocytosis and phagocytosis by macrophages. *J. Cell Biol.* 135:1249–1260. http://dx.doi.org/10.1083/jcb.135.5.1249

Aymard, E., V. Barruche, T. Naves, S. Bordes, B. Closs, M. Verdier, and M.H. Ratinaud. 2011. Autophagy in human keratinocytes: An early step of the differentiation? *Exp. Dermatol.* 20:263–268. http://dx.doi.org/10.1111/j.1600-0625.2010.01157.x

Barrandon, Y., and H. Green. 1987. Three clonal types of keratinocyte with different capacities for multiplication. *Proc. Natl. Acad. Sci. USA.* 84:2302–2306. http://dx.doi.org/10.1073/pnas.84.8.2302

Barth, S., D. Glick, and K.F. Macleod. 2010. Autophagy: Assays and artifacts. *J. Pathol.* 221:117–124. http://dx.doi.org/10.1002/path.2694

Bell, B.D., S. Leverrier, B.M. Weist, R.H. Newton, A.F. Arechiga, K.A. Luhrs, N.S. Morrissette, and C.M. Walsh. 2008. FADD and caspase-8 control the outcome of autophagic signaling in proliferating T cells. *Proc. Natl. Acad. Sci. USA.* 105:16677–16682. http://dx.doi.org/10.1073/pnas.0808597105

Bjørkøy, G., T. Lamark, A. Brech, H. Outzen, M. Perander, A. Overvatn, H. Stenmark, and T. Johansen. 2005. p62/SQSTM1 forms protein aggregates degraded by autophagy and has a protective effect on huntingtin-induced cell death. *J. Cell Biol.* 171:603–614. http://dx.doi.org/10.1083/jcb.200507002

Blanpain, C., and E. Fuchs. 2009. Epidermal homeostasis: A balancing act of stem cells in the skin. *Nat. Rev. Mol. Cell Biol.* 10:207–217. http://dx.doi.org/10.1038/nrm2636

Boya, P., R.A. Gonzalez-Polo, D. Poncet, K. Andreau, H.L. Vieira, T. Roumier, J.L. Perfettini, and G. Kroemer. 2003. Mitochondrial membrane permeabilization is a critical step of lysosome-initiated apoptosis induced by hydroxychloroquine. *Oncogene.* 22:3927–3936. http://dx.doi.org/10.1038/sj.onc.1206622

Bradbury, P., C.T. Bach, A. Paul, and G.M. O'Neill. 2014. Src kinase determines the dynamic exchange of the docking protein NEDD9 (neural precursor cell expressed developmentally down-regulated gene 9) at focal adhesions. *J. Biol. Chem.* 289:24792–24800. http://dx.doi.org/10.1074/jbc.M113.544106

Caplan, S., L.M. Hartnell, R.C. Aguilar, N. Naslavsky, and J.S. Bonifacino. 2001. Human Vam6p promotes lysosome clustering and fusion in vivo. *J. Cell Biol.* 154:109–122. http://dx.doi.org/10.1083/jcb.200102142

Chen, Y., and L. Yu. 2013. Autophagic lysosome reformation. *Exp. Cell Res.* 319:142–146. http://dx.doi.org/10.1016/j.yexcr.2012.09.004

Chen, N., N. Eritja, R. Lock, and J. Debnath. 2013. Autophagy restricts proliferation driven by oncogenic phosphatidylinositol 3-kinase in three-dimensional culture. *Oncogene.* 32:2543–2554. http://dx.doi.org/10.1038/onc.2012.277

Chen, P.M., Z.J. Gombart, and J.W. Chen. 2011. Chloroquine treatment of ARPE-19 cells leads to lysosome dilation and intracellular lipid accumulation: Possible implications of lysosomal dysfunction in macular degeneration. *Cell Biosci.* 1:10. http://dx.doi.org/10.1186/2045-3701-1-10

Chua, C.E., B.Q. Gan, and B.L. Tang. 2011. Involvement of members of the Rab family and related small GTPases in autophagosome formation and maturation. *Cell. Mol. Life Sci.* 68:3349–3358. http://dx.doi.org/10.1007/s00018-011-0748-9

Cianfanelli, V., M. D'Orazio, and F. Cecconi. 2015. AMBRA1 and BECLIN 1 interplay in the crosstalk between autophagy and cell proliferation. *Cell Cycle.* 14:959–963. http://dx.doi.org/10.1080/15384101.2015.1021526

Commisso, C., S.M. Davidson, R.G. Soydaner-Azeloglu, S.J. Parker, J.J. Kamphorst, S. Hackett, E. Grabocka, M. Nofal, J.A. Drebin, C.B. Thompson, et al. 2013. Macropinocytosis of protein is an amino acid supply route in Ras-transformed cells. *Nature.* 497:633–637. http://dx.doi.org/10.1038/nature12138

Cotsarelis, G., S.Z. Cheng, G. Dong, T.-T. Sun, and R.M. Lavker. 1989. Existence of slow-cycling limbal epithelial basal cells that can be preferentially stimulated to proliferate: Implications on epithelial stem cells. *Cell.* 57:201–209. http://dx.doi.org/10.1016/0092-8674(89)90958-6

Cousin, M.A., and P.J. Robinson. 2001. The dephosphins: Dephosphorylation by calcineurin triggers synaptic vesicle endocytosis. *Trends Neurosci.* 24:659–665. http://dx.doi.org/10.1016/S0166-2236(00)01930-5

Davies, S.B., and N. Di Girolamo. 2010. Corneal stem cells and their origins: Significance in developmental biology. *Stem Cells Dev.* 19:1651–1662. http://dx.doi.org/10.1089/scd.2010.0201

Eskelinen, E.L., and P. Saftig. 2009. Autophagy: a lysosomal degradation pathway with a central role in health and disease. *Biochim. Biophys. Acta.* 1793:664–673. http://dx.doi.org/10.1016/j.bbamcr.2008.07.014

Florey, O., S.E. Kim, C.P. Sandoval, C.M. Haynes, and M. Overholtzer. 2011. Autophagy machinery mediates macroendocytic processing and entotic cell death by targeting single membranes. *Nat. Cell Biol.* 13:1335–1343. http://dx.doi.org/10.1038/ncb2363

Freundt, E.C., M. Czapiga, and M.J. Lenardo. 2007. Photoconversion of Lysotracker Red to a green fluorescent molecule. *Cell Res.* 17:956–958. http://dx.doi.org/10.1038/cr.2007.80

Guan, J.L., A.K. Simon, M. Prescott, J.A. Menendez, F. Liu, F. Wang, C. Wang, E. Wolvetang, A. Vazquez-Martin, and J. Zhang. 2013. Autophagy in stem cells. *Autophagy.* 9:830–849. http://dx.doi.org/10.4161/auto.24132

Gukovskaya, A.S., and I. Gukovsky. 2012. Autophagy and pancreatitis. *Am. J. Physiol. Gastrointest. Liver Physiol.* 303:G993–G1003. http://dx.doi.org/10.1152/ajpgi.00122.2012

Ha, S.D., B. Ham, J. Mogridge, P. Saftig, S. Lin, and S.O. Kim. 2010. Cathepsin B-mediated autophagy flux facilitates the anthrax toxin receptor 2-mediated delivery of anthrax lethal factor into the cytoplasm. *J. Biol. Chem.* 285:2120–2129. http://dx.doi.org/10.1074/jbc.M109.065813

He, C., M.C. Bassik, V. Moresi, K. Sun, Y. Wei, Z. Zou, Z. An, J. Loh, J. Fisher, Q. Sun, et al. 2012. Exercise-induced BCL2-regulated autophagy is required for muscle glucose homeostasis. *Nature.* 481:511–515. http://dx.doi.org/10.1038/nature10758

Jens, M., and N. Rajewsky. 2015. Competition between target sites of regulators shapes post-transcriptional gene regulation. *Nat. Rev. Genet.* 16:113–126. http://dx.doi.org/10.1038/nrg3853

Juopperi, T.A., W.R. Kim, C.H. Chiang, H. Yu, R.L. Margolis, C.A. Ross, G.L. Ming, and H. Song. 2012. Astrocytes generated from patient induced pluripotent stem cells recapitulate features of Huntington's disease patient cells. *Mol. Brain.* 5:17. http://dx.doi.org/10.1186/1756-6606-5-17

Kitambi, S.S., E.M. Toledo, D. Usoskin, S. Wee, A. Harisankar, R. Svensson, K. Sigmundsson, C. Kalderén, M. Niklasson, S. Kundu, et al. 2014. Vulnerability of glioblastoma cells to catastrophic vacuolization and death induced by a small molecule. *Cell.* 157:313–328. http://dx.doi.org/10.1016/j.cell.2014.02.021

Klionsky, D.J., F.C. Abdalla, H. Abeliovich, R.T. Abraham, A. Acevedo-Arozena, K. Adeli, L. Agholme, M. Agnello, P. Agostinis, J.A. Aguirre-Ghiso, et al. 2012. Guidelines for the use and interpretation of assays for monitoring autophagy. *Autophagy.* 8:445–544. http://dx.doi.org/10.4161/auto.19496

Koivusalo, M., C. Welch, H. Hayashi, C.C. Scott, M. Kim, T. Alexander, N. Touret, K.M. Hahn, and S. Grinstein. 2010. Amiloride inhibits macropinocytosis by lowering submembranous pH and preventing Rac1 and Cdc42 signaling. *J. Cell Biol.* 188:547–563. http://dx.doi.org/10.1083/jcb.200908086

Krishna, S., and X. Zhong. 2013. Role of diacylglycerol kinases in T cell development and function. *Crit. Rev. Immunol.* 33:97–118. http://dx.doi.org/10.1615/CritRevImmunol.2013006696

Lamb, C.A., T. Yoshimori, and S.A. Tooze. 2013. The autophagosome: Origins unknown, biogenesis complex. *Nat. Rev. Mol. Cell Biol.* 14:759–774. http://dx.doi.org/10.1038/nrm3696

Lavker, R.M. 1979. Structural alterations in exposed and unexposed aged skin. *J. Invest. Dermatol.* 73:59–66. http://dx.doi.org/10.1111/1523-1747.ep12532763

Lavker, R.M., and T.-T. Sun. 2000. Epidermal stem cells: Properties, markers, and location. *Proc. Natl. Acad. Sci. USA.* 97:13473–13475. http://dx.doi.org/10.1073/pnas.250380097

Lavker, R.M., G. Dong, S.Z. Cheng, K. Kudoh, G. Cotsarelis, and T.T. Sun. 1991. Relative proliferative rates of limbal and corneal epithelia. Implications of corneal epithelial migration, circadian rhythm, and suprabasally located DNA-synthesizing keratinocytes. *Invest. Ophthalmol. Vis. Sci.* 32:1864–1875.

Lavker, R.M., Z.G. Wei, and T.T. Sun. 1998. Phorbol ester preferentially stimulates mouse fornical conjunctival and limbal epithelial cells to proliferate in vivo. *Invest. Ophthalmol. Vis. Sci.* 39:301–307.

Lavker, R.M., S.C.G. Tseng, and T.-T. Sun. 2004. Corneal epithelial stem cells at the limbus: Looking at some old problems from a new angle. *Exp. Eye Res.* 78:433–446. http://dx.doi.org/10.1016/j.exer.2003.09.008

Lehrer, M.S., T.T. Sun, and R.M. Lavker. 1998. Strategies of epithelial repair: Modulation of stem cell and transit amplifying cell proliferation. *J. Cell Sci.* 111:2867–2875.

Lewis, W. 1931. Pinocytosis. *Johns Hopkins Hosp Bull.* 49:17–27.

Li, M.D., D. Sun, X.Y. Lou, J. Beuten, T.J. Payne, and J.Z. Ma. 2007. Linkage and association studies in African- and Caucasian-American populations demonstrate that SHC3 is a novel susceptibility locus for nicotine dependence. *Mol. Psychiatry.* 12:462–473. http://dx.doi.org/10.1038/sj.mp.4001933

Li, Y., T. Inoue, F. Takamatsu, T. Kobayashi, A. Shiraishi, N. Maeda, Y. Ohashi, and K. Nishida. 2014. Differences between niche cells and limbal stromal cells in maintenance of corneal limbal stem cells. *Invest. Ophthalmol. Vis. Sci.* 55:1453–1462. http://dx.doi.org/10.1167/iovs.13-13698

Lim, J.P., and P.A. Gleeson. 2011. Macropinocytosis: An endocytic pathway for internalising large gulps. *Immunol. Cell Biol.* 89:836–843. http://dx.doi.org/10.1038/icb.2011.20

Ling, D., and P.M. Salvaterra. 2011. Brain aging and $A\beta_{1-42}$ neurotoxicity converge via deterioration in autophagy-lysosomal system: A conditional *Drosophila* model linking Alzheimer's neurodegeneration with aging. *Acta Neuropathol.* 121:183–191. http://dx.doi.org/10.1007/s00401-010-0772-0

Liu, J., Y. Lv, Q.H. Liu, C.K. Qu, and J. Shen. 2014. Deficiency of MTMR14 promotes autophagy and proliferation of mouse embryonic fibroblasts. *Mol. Cell. Biochem.* 392:31–37. http://dx.doi.org/10.1007/s11010-014-2015-5

Maltese, W.A., and J.H. Overmeyer. 2015. Non-apoptotic cell death associated with perturbations of macropinocytosis. *Front. Physiol.* 6:38. http://dx.doi.org/10.3389/fphys.2015.00038

Martinet, W., M.W. Knaapen, M.M. Kockx, and G.R. De Meyer. 2007. Autophagy in cardiovascular disease. *Trends Mol. Med.* 13:482–491. http://dx.doi.org/10.1016/j.molmed.2007.08.004

Mettlen, M., A. Platek, P. Van Der Smissen, S. Carpentier, M. Amyere, L. Lanzetti, P. de Diesbach, D. Tyteca, and P.J. Courtoy. 2006. Src triggers circular ruffling and macropinocytosis at the apical surface of polarized MDCK cells. *Traffic.* 7:589–603. http://dx.doi.org/10.1111/j.1600-0854.2006.00412.x

Minna, E., P. Romeo, L. De Cecco, M. Dugo, G. Cassinelli, S. Pilotti, D. Degl'Innocenti, C. Lanzi, P. Casalini, M.A. Pierotti, et al. 2014. miR-199a-3p displays tumor suppressor functions in papillary thyroid carcinoma. *Oncotarget.* 5:2513–2528. http://dx.doi.org/10.18632/oncotarget.1830

Mizushima, N., A. Yamamoto, M. Matsui, T. Yoshimori, and Y. Ohsumi. 2004. In vivo analysis of autophagy in response to nutrient starvation using transgenic mice expressing a fluorescent autophagosome marker. *Mol. Biol. Cell.* 15:1101–1111. http://dx.doi.org/10.1091/mbc.E03-09-0704

Mizushima, N., T. Yoshimori, and B. Levine. 2010. Methods in mammalian autophagy research. *Cell.* 140:313–326. http://dx.doi.org/10.1016/j.cell.2010.01.028

Moncini, S., A. Salvi, P. Zuccotti, G. Viero, A. Quattrone, S. Barlati, G. De Petro, M. Venturin, and P. Riva. 2011. The role of miR-103 and miR-107 in regulation of CDK5R1 expression and in cellular migration. *PLoS One.* 6:e20038. http://dx.doi.org/10.1371/journal.pone.0020038

Mortensen, M., E.J. Soilleux, G. Djordjevic, R. Tripp, M. Lutteropp, E. Sadighi-Akha, A.J. Stranks, J. Glanville, S. Knight, S.E. Jacobsen, et al. 2011. The autophagy protein Atg7 is essential for hematopoietic stem cell maintenance. *J. Exp. Med.* 208:455–467. http://dx.doi.org/10.1084/jem.20101145

O'Neill, G.M., S.J. Fashena, and E.A. Golemis. 2000. Integrin signalling: A new Cas(t) of characters enters the stage. *Trends Cell Biol.* 10:111–119. http://dx.doi.org/10.1016/S0962-8924(99)01714-6

Oliver, L., E. Hue, M. Priault, and F.M. Vallette. 2012. Basal autophagy decreased during the differentiation of human adult mesenchymal stem cells. *Stem Cells Dev.* 21:2779–2788. http://dx.doi.org/10.1089/scd.2012.0124

Overmeyer, J.H., A.M. Young, H. Bhanot, and W.A. Maltese. 2011. A chalcone-related small molecule that induces methuosis, a novel form of non-apoptotic cell death, in glioblastoma cells. *Mol. Cancer.* 10:69. http://dx.doi.org/10.1186/1476-4598-10-69

Palm, W., Y. Park, K. Wright, N.N. Pavlova, D.A. Tuveson, and C.B. Thompson. 2015. The utilization of extracellular proteins as nutrients is suppressed by mTORC1. *Cell.* 162:259–270. http://dx.doi.org/10.1016/j.cell.2015.06.017

Peng, H., N. Kaplan, R.B. Hamanaka, J. Katsnelson, H. Blatt, W. Yang, L. Hao, P.J. Bryar, R.S. Johnson, S. Getsios, et al. 2012. microRNA-31/factor-inhibiting hypoxia-inducible factor 1 nexus regulates keratinocyte differentiation. *Proc. Natl. Acad. Sci. USA.* 109:14030–14034. http://dx.doi.org/10.1073/pnas.1111292109

Peng, H., J.K. Park, J. Katsnelson, N. Kaplan, W. Yang, S. Getsios, and R.M. Lavker. 2015. microRNA-103/107 family regulates multiple epithelial stem cell characteristics. *Stem Cells.* 33:1642–1656. http://dx.doi.org/10.1002/stem.1962

Phadwal, K., A.S. Watson, and A.K. Simon. 2013. Tightrope act: Autophagy in stem cell renewal, differentiation, proliferation, and aging. *Cell. Mol. Life Sci.* 70:89–103. http://dx.doi.org/10.1007/s00018-012-1032-3

Potten, C.S., and M. Loeffler. 1990. Stem cells: Attributes, cycles, spirals, pitfalls and uncertainties. Lessons for and from the crypt. *Development.* 110:1001–1020.

Powell, K.A., V.A. Valova, C.S. Malladi, O.N. Jensen, M.R. Larsen, and P.J. Robinson. 2000. Phosphorylation of dynamin I on Ser-795 by protein kinase C blocks its association with phospholipids. *J. Biol. Chem.* 275:11610–11617. http://dx.doi.org/10.1074/jbc.275.16.11610

Qu, X., J. Yu, G. Bhagat, N. Furuya, H. Hibshoosh, A. Troxel, J. Rosen, E.L. Eskelinen, N. Mizushima, Y. Ohsumi, et al. 2003. Promotion of tumorigenesis by heterozygous disruption of the beclin 1 autophagy gene. *J. Clin. Invest.* 112:1809–1820. http://dx.doi.org/10.1172/JCI20039

Ramírez-Valle, F., S. Braunstein, J. Zavadil, S.C. Formenti, and R.J. Schneider. 2008. eIF4GI links nutrient sensing by mTOR to cell proliferation and inhibition of autophagy. *J. Cell Biol.* 181:293–307. http://dx.doi.org/10.1083/jcb.200710215

Rohrer, J., A. Schweizer, D. Russell, and S. Kornfeld. 1996. The targeting of Lamp1 to lysosomes is dependent on the spacing of its cytoplasmic tail tyrosine sorting motif relative to the membrane. *J. Cell Biol.* 132:565–576. http://dx.doi.org/10.1083/jcb.132.4.565

Salemi, S., S. Yousefi, M.A. Constantinescu, M.F. Fey, and H.U. Simon. 2012. Autophagy is required for self-renewal and differentiation of adult human stem cells. *Cell Res.* 22:432–435. http://dx.doi.org/10.1038/cr.2011.200

Sanghi, S., R. Kumar, A. Lumsden, D. Dickinson, V. Klepeis, V. Trinkaus-Randall, H.F. Frierson Jr., and G.W. Laurie. 2001. cDNA and genomic cloning of lacritin, a novel secretion enhancing factor from the human lacrimal gland. *J. Mol. Biol.* 310:127–139. http://dx.doi.org/10.1006/jmbi.2001.4748

Schermer, A., S. Galvin, and T.-T. Sun. 1986. Differentiation-related expression of a major 64K corneal keratin in vivo and in culture suggests limbal location of corneal epithelial stem cells. *J. Cell Biol.* 103:49–62. http://dx.doi.org/10.1083/jcb.103.1.49

Schlötzer-Schrehardt, U., and F.E. Kruse. 2005. Identification and characterization of limbal stem cells. *Exp. Eye Res.* 81:247–264. http://dx.doi.org/10.1016/j.exer.2005.02.016

Schnatwinkel, C., S. Christoforidis, M.R. Lindsay, S. Uttenweiler-Joseph, M. Wilm, R.G. Parton, and M. Zerial. 2004. The Rab5 effector Rabankyrin-5 regulates and coordinates different endocytic mechanisms. *PLoS Biol.* 2:E261. http://dx.doi.org/10.1371/journal.pbio.0020261

Shen, H.M., and N. Mizushima. 2014. At the end of the autophagic road: An emerging understanding of lysosomal functions in autophagy. *Trends Biochem. Sci.* 39:61–71. http://dx.doi.org/10.1016/j.tibs.2013.12.001

Stepp, M.A., and J.D. Zieske. 2005. The corneal epithelial stem cell niche. *Ocul. Surf.* 3:15–26. http://dx.doi.org/10.1016/S1542-0124(12)70119-2

Sun, T.T., S.C. Tseng, and R.M. Lavker. 2010. Location of corneal epithelial stem cells. *Nature.* 463:E10–E11. http://dx.doi.org/10.1038/nature08805

Tang, A.H., and T.A. Rando. 2014. Induction of autophagy supports the bioenergetic demands of quiescent muscle stem cell activation. *EMBO J.* 33:2782–2797. http://dx.doi.org/10.15252/embj.201488278

Tomizawa, K., S. Sunada, Y.F. Lu, Y. Oda, M. Kinuta, T. Ohshima, T. Saito, F.Y. Wei, M. Matsushita, S.T. Li, et al. 2003. Cophosphorylation of amphiphysin I and dynamin I by Cdk5 regulates clathrin-mediated endocytosis of synaptic vesicles. *J. Cell Biol.* 163:813–824. http://dx.doi.org/10.1083/jcb.200308110

Veithen, A., P. Cupers, P. Baudhuin, and P.J. Courtoy. 1996. v-Src induces constitutive macropinocytosis in rat fibroblasts. *J. Cell Sci.* 109: 2005–2012.

Vessoni, A.T., A.R. Muotri, and O.K. Okamoto. 2012. Autophagy in stem cell maintenance and differentiation. *Stem Cells Dev.* 21:513–520. http://dx.doi.org/10.1089/scd.2011.0526

Wang, N., K. Zimmerman, R.W. Raab, R.L. McKown, C.M. Hutnik, V. Talla, M.F. Tyler IV, J.K. Lee, and G.W. Laurie. 2013. Lacritin rescues stressed epithelia via rapid forkhead box O3 (FOXO3)-associated autophagy that restores metabolism. *J. Biol. Chem.* 288:18146–18161. http://dx.doi.org/10.1074/jbc.M112.436584

Wei, Z.G., R.L. Wu, R.M. Lavker, and T.T. Sun. 1993. In vitro growth and differentiation of rabbit bulbar, fornix, and palpebral conjunctival epithelia. Implications on conjunctival epithelial transdifferentiation and stem cells. *Invest. Ophthalmol. Vis. Sci.* 34:1814–1828.

Wei, Z.G., T. Lin, T.T. Sun, and R.M. Lavker. 1997. Clonal analysis of the in vivo differentiation potential of keratinocytes. *Invest. Ophthalmol. Vis. Sci.* 38:753–761.

West, M.A., A.R. Prescott, E.L. Eskelinen, A.J. Ridley, and C. Watts. 2000. Rac is required for constitutive macropinocytosis by dendritic cells but does not control its downregulation. *Curr. Biol.* 10:839–848. http://dx.doi.org/10.1016/S0960-9822(00)00595-9

Wu, W.K., Y.C. Wu, L. Yu, Z.J. Li, J.J. Sung, and C.H. Cho. 2008. Induction of autophagy by proteasome inhibitor is associated with proliferative arrest in colon cancer cells. *Biochem. Biophys. Res. Commun.* 374:258–263. http://dx.doi.org/10.1016/j.bbrc.2008.07.031

Yamamoto, A., Y. Tagawa, T. Yoshimori, Y. Moriyama, R. Masaki, and Y. Tashiro. 1998. Bafilomycin A1 prevents maturation of autophagic vacuoles by inhibiting fusion between autophagosomes and lysosomes in rat hepatoma cell line, H-4-II-E cells. *Cell Struct. Funct.* 23:33–42. http://dx.doi.org/10.1247/csf.23.33

Yazdankhah, M., S. Farioli-Vecchioli, A.B. Tonchev, A. Stoykova, and F. Cecconi. 2014. The autophagy regulators Ambra1 and Beclin 1 are required for adult neurogenesis in the brain subventricular zone. *Cell Death Dis.* 5:e1403. http://dx.doi.org/10.1038/cddis.2014.358

Yoshimori, T., A. Yamamoto, Y. Moriyama, M. Futai, and Y. Tashiro. 1991. Bafilomycin A1, a specific inhibitor of vacuolar-type H(+)-ATPase, inhibits acidification and protein degradation in lysosomes of cultured cells. *J. Biol. Chem.* 266:17707–17712.

Yu, J., D. Ryan, S. Getsios, M. Oliveira-Fernandes, A. Fatima, and R. Lavker. 2008. MicroRNA-184 antagonizes microRNA-205 to maintain SHIP2 levels in epithelia. *Proc. Natl. Acad. Sci. USA.* 105:19300–19305. http://dx.doi.org/10.1073/pnas.0803992105

Yu, L., C.K. McPhee, L. Zheng, G.A. Mardones, Y. Rong, J. Peng, N. Mi, Y. Zhao, Z. Liu, F. Wan, et al. 2010. Termination of autophagy and reformation of lysosomes regulated by mTOR. *Nature.* 465:942–946. http://dx.doi.org/10.1038/nature09076

Zhou, M., X.M. Li, and R.M. Lavker. 2006. Transcriptional profiling of enriched populations of stem cells versus transient amplifying cells. A comparison of limbal and corneal epithelial basal cells. *J. Biol. Chem.* 281:19600–19609. http://dx.doi.org/10.1074/jbc.M600777200